SEMI-VOLATILE ORGANIC COMPOUNDS: BEHAVIOR AND SECONDARY ORGANIC AEROSOL FORMATION

Penglin Ye

Center for Atmospheric Particle Studies

Chemistry Department

Carnegie Mellon University

Pittsburgh, Pennsylvania

February 2015

In partial fulfillment of the requirements for the Ph.D. degree in Chemistry

ABSTRACT

This thesis mainly described the development of studying the behavior and secondary organic aerosol formation from semi-volatile organic compounds (SVOCs). SVOCs comprises a significant fraction of the organic mass in particulate matter (PM), which has shown important impacts on human health and also influences on Earth's climate. SVOCs are thought to play essential roles in the formation of SOA, chemical aging and mixing processes. Smog chambers have been extensively used to study SOA formation, chemical reaction and physical properties. The interaction between SVOC vapor with Teflon chamber wall and suspended particles is a key factor influencing organic aerosol formations and behaviors in chamber experiments. We observed that pinanediol (PD) showed a large chamber wall deposition and reached a steady concentration, only around 14% of mass left in the gas phase. But we did not observe the release of PD from the chamber walls during isothermal dilution of the chamber with fresh air at 22 ^{o}C, which indicated there was no PD released from the chamber walls during the SOA formation. This clearly shows the vapor loss of SVOC precursors need to be considered when studying their SOA formation. The average carbon oxidation states the SOA from PD were calculated as around -0.7, which were similar to the value observed in CLOUD. Our data are consistent with ~10% of the SOA with low volatility that could drive new particle formation. It is challenging to measure SVOC vapor concentrations and properties. A new approach is discussed in this thesis, studying SVOC vapors from measuring the particles. The SVOCs coated particles sustained the SVOCs in the gas phase at or near their saturation concentration. The mass loss of SVOCs from the suspended particles thus reflects SVOCs vapor wall loss. Our results show the vapor wall

loss rate of SVOC is consistently proportional to the SVOC vapor concentrations. We observed PEG400 seeds can sorb semi-volatile α-pinene SOA vapors. This allows us to trap semi-volatile α-pinene SOA into PEG400 seeds and then analyze their compositions and properties through measuring particles. PEG400 is liquid, water-soluble, nearly non-volatile, good solvent for SOA and relative stable during the oxidation with OH radicals and ozone. It can also be easily separated from the SOA mass spectrum with the unique fragment $C_4H_9O_2^+$ at m/z=89. The results demonstrated that SOA prepared from α-pinene reacted with OH produced more semi-volatile SOA vapors comparing to α-pinene ozonolysis. More semi-volatile SOA vapors were observed in the gas phase with higher SOA loadings. With well-built particle measurement methods, we may get more knowledge on the SVOC vapors.

ACKNOWLEDGEMENTS

This thesis is dedicated to my parents, Yujuan Chi and Xueyu Ye, for their unconditional love and support, through my life in United States.

I owe my deepest gratitude to my advisor, Prof. Neil M. Donahue, for all he has done for me during my PhD study. This dissertation would not have been possible without him. For four years, he is always accessible and willing to offer invaluable assistance, support and guidance for my research. He sets an example for me as a world-class researcher with tremendous passion, creativity and knowledge on science. His passions and working styles stimulated my pursuit of knowledge in the field of atmospheric science. In addition, he kindly gave me a hand every time when I asked for a favor.

I would like to acknowledge my advisory committee members, Prof. Rongchao Jin, for his insightful discussions and supports about my study and research projects; and Prof. Ryan C. Sullivan, for his patient explanations and inspired suggestions on my projects. I would like to thank Prof. Peter J. Adams for his kindness to serve on my thesis committee and also his great courses.

I would like to acknowledge the faculty members in CAPS, Prof. Spyros N. Pandis, Prof. Allen L. Robinson, and Prof. Albert A. Presto for their very helpful instructions on my PhD study. I would like to thank Prof. Jasper Kirkby for the leading and instructions during the CLOUD7 campaign.

I appreciate all my collaborators, for their supports on the measurement and their advices in my research projects. I had inspired and helpful discussions in the collaborations with

Dr. Heber Chacon-Madrid, Dr. Yunliang Zhao, Dr. Wayne Chuang, Dr. Rawad Saleh, Dr. Xiang Ding, Jani Hakala, Dr. Ellis Robinson, Qing Ye, Victoria Hofbauer, Dr. Yi Tan, Dr. Jonathan Duplissy and all CLOUD 7 Team.

It is a great honor for me to work with many talented scientists in CAPS. Many group members have collaborated and helped me with my projects. I especially thank Prof. Eric Lipsky for managing the lab. I appreciate all the CAPSians for the helpful discussion and support to my research projects.

I would like to especially acknowledge Dr. Rea Freeland for the help during the transition. I would like to thank Valerie Bridge, Sara Wainer and many other people in Chemistry for arranging the defense and a lot of help during my PhD study.

I am grateful to all of the group members, graduate students, staff and faculty members in Chemistry and all my friends. Their kind help and friendship let me enjoy the life in US.

TABLE OF CONTENTS

LIST OF SCHEMES

LIST OF FIGURES

Chapter 1

Introduction

1.1 Aerosols and secondary organic aerosols

Aerosols are solid or liquid particles suspended in the atmosphere. The particle sizes in aerosol range from nanometers to micrometers in diameter. In most situations, aerosols can be used interchangeably with another term: "particulate matter (PM)". PM2.5 concentrations are widely used today to indicate air quality. Aerosols in the atmosphere affect the climate by absorbing and scattering solar radiation, and by altering the properties and lifetimes of clouds (Solomon, 2007). It has also been implicated in human disease and mortality (Pope et al., 2009).

The effects of aerosols on climate change include direct and indirect effects when considering radiative forcing of the climate system. Radiative forcings are changes in the net energy fluxes in the atmosphere, which include solar radiation and terrestrial radiation. Direct effects are the scattering and absorption of radiation by aerosol particles. Indirect effects influence climate through: changes in the cloud condensation nuclei (CCN) activity, which affect clouds and precipitation; or changes in overall chemical and biological activity, which affects aerosol and trace gas emissions and transformation. As a result, aerosols markedly affect the radiative balance in Earth's atmosphere and play an important role in climate (Solomon, 2007).

Atmospheric aerosols also have an important impact on human health. It is now well established that exposure to ambient aerosols is associated with damaging effects on the respiratory and cardiovascular systems (Pope and Dockery, 2006). Fine particles—particles smaller than 2.5 μm—are proposed to be harmful to human health based on their sufficiently small size longer

retention time, allowing them to penetrate the membranes of the respiratory tract and enter the circulatory system (Oberdörster et al., 2004). Exposure to fine particles has been associated with increased morbidity and mortality; consequently, sustained reductions in pollution exposure result in improved life expectancy. A decrease of 10 μg cm^{-3} in fine particle concentration resulted in an estimated increase in mean life expectancy of 0.61 year (Pope et al., 2009).

Aerosols arise directly from emissions of particles and also from the conversion of certain gases to particles in the atmosphere. Different types of chemical species are emitted into the atmosphere constantly and are categorized as either anthropogenic (arising from human activities) or biogenic (arising from natural resources, such as vegetation). Aerosols may also be categorized as primary or secondary. Primary particles are directly emitted from sources. The major sources include biomass burning, combustion of fossil fuels, volcanic eruptions and wind-driven suspension of soil, mineral dust, sea salt and biological materials. Secondary particles are formed by species in the gas phase through nucleation, condensation, and heterogeneous and multiphase chemical reactions. The conversion of inorganic gases such as sulfur dioxide, nitrogen dioxide and ammonia into particulate phase sulfate, nitrate and ammonium is now fairly well understood. Inorganic emissions remain relatively stable during their travel in the atmosphere. However, the oxidation of organic material in the atmosphere is much more dynamic due to constant photo-oxidation and changes in thermodynamic properties (Seinfeld and Pandis, 2006). Some organic species can partition between gas-phase and aerosol phase. Those organic compounds experience direct chemical transformation after reaction with the OH radical, ozone, and the nitrate radical, which are the three major oxidants. Both the oxidation state and the volatility of the products change with each reaction. The oxidized products will partition into

the particle phase or generate new particles, forming secondary organic aerosol (SOA) (Donahue et al., 2006).

1.2 Oxidation of SOA precursors

The formation of SOA starts with the oxidation of volatile organic compound (VOC) precursors by hydroxyl (OH) radicals, ozone (O_3), nitrate (NO_3) radicals (Kroll and Seinfeld, 2008). Under certain conditions in the marine atmosphere, chlorine atoms (Cl) may also initiate the oxidation of VOCs. The major VOC precursors in the atmosphere include aromatic compounds (e.g. toluene, xylene), isoprene, monoterpenes (e.g. α-pinene) and sesquiterpenes (e.g. β-caryophyllene).

Ozone reacts with and cleaves carbon-carbon double bonds (C=C) in the molecules and forms ketones, aldehydes or acids, which contain carbonyl groups (C=O). Criegee intermediate is one of the stable intermediate products formed during the reaction.

Two important steps in the oxidation of VOCs by OH radicals are hydrogen atom abstraction and addition of O_2 (Seinfeld and Pankow, 2003). OH radicals have high reactivity, and easily grab a hydrogen atom from organic molecules to leave alkyl radicals (R·). Alkyl radicals will then quickly react with O_2 and form peroxide radicals (ROO·), a relatively stable species. (Due to abundant O_2 in the atmosphere (21%), the lifetime of alkyl radicals is very short.) NO in the atmosphere will then convert ROO· to an alkoxy radical (RO·). RO· may undergo isomerization (abstract another hydrogen atom from another carbon and generate a new alkyl radical) or become a stable species: alcohol, ketone or aldehydes.

Compared to the OH radical, NO_3 is less likely to abstract a hydrogen atom, but prefers to attack carbon-carbon double bonds (C=C) that lead to an addition reaction and form alkyl radicals (R·).

The relative importance of these competing oxidation depends on the structure of the VOC and on the ambient conditions (Atkinson and Arey, 2003). The initial oxidation step produces a series of organic products containing one or more polar oxygenated functional groups including aldehyde (−C(=O)H), ketone (−C(=O)−), alcohol (−OH), nitrate ($-ONO_2$), peroxyacyl nitrate ($-C(=O)OONO_2$), carboxylic acid (−C(=O)OH), hydroperoxide (−OOH) and percarboxylic acid (−C(=O)OOH) groups (Hallquist et al., 2009). These functional groups tend to increase van der Waals force between the oxidation products and make the products less volatile and more water soluble. Further oxidation of the products may add more functional groups, such that the "second-generation" oxidation may be even lower in volatility and more water soluble. Functionality is used to describe these pathways that add functional groups into the products, while fragmentation describes a simultaneous oxidation mechanism that leads to the cleavage of the carbon chains to form molecules with smaller carbon numbers. The products usually have lower molecular weight (MW) and are more volatile, so they tend to stay in the gas phase and not contribute to SOA formation directly. When given enough time to allow oxidation to continue, all the carbon in the emitted VOCs would be ultimately converted into CO_2. Besides oxidation, the precursors and oxidation products may undergo oligomerization, also termed as accretion reactions (Barsanti and Pankow, 2006), by combining two or more molecules together. The formation of an oligomer comes with a dramatic decrease in volatility. Because of the complexity of the emitted VOC mixture and the numerous combinations of oxidation mechanisms on each carbon on an organic molecule, the organic population in the atmosphere contains many thousands of different organic oxygenates, which possess a wide range of properties, such as reactivity, volatility, and aqueous solubility. It is estimated that more than 10,000 different organic compounds have been detected in the atmosphere (Goldstein and

Galbally, 2007). Ambient conditions such as NOx level and relative humidity (RH) affect the oxidation mechanism and change the distribution of products formed, and therefore influence the SOA formation from a given precursor. Each VOC may undergo a number of chemical reactions to produce a series of new oxidized products, which may or may not contribute to SOA formation and growth or further chemical evolution. This further increases the complexity of the situation.

1.3 Gas-particle partitioning theory

VOCs in the atmosphere produce a series of oxygenated organic products through chemical reactions, mostly through oxidation and oligomerization. Aerosols comprise a very wide range of compounds, and far too few are identified. As a consequence, aggregate characteristics are used to study organic aerosol in the model simulations. Volatility, as also called saturation concentration, is one of these important parameters. Organic species with low volatility can easily partition into the particle phase by forming a new particle or condensing to the existing particles, thus forming SOA. The SOA contribution of given an organic species is mostly determined by its volatility. The saturation concentration (C^*), with the units $\mu g\ m^{-3}$, is used to describe the volatility. Based on the volatility the organic species can be categorized as: (Donahue et al., 2012b)

– Extremely low volatility organic compounds (ELVOC, $C^* < 3\times10^{-4}\ \mu g\ m^{-3}$). ELVOC are almost entirely in the particle phase under any ambient condition

– Low volatility organic compounds (LVOC, $3\times10^{-4} < C^* < 0.3\ \mu g\ m^{-3}$). These are predominantly in the particle phase in the atmosphere.

– Semi-volatile organic compounds (SVOC, $0.3 < C^* < 300$ μg m^{-3}). These compounds can be in either phase but often have sizable mass fractions in both phases. They comprise the major part of organic compounds studies in the thesis.

– Intermediate volatility organic compounds (IVOC, $300 < C^* < 3\times10^6$ μg m^{-3}). Myriad compounds of quite low vapor pressure that nonetheless reside almost exclusively in the gas phase under atmospheric conditions (Robinson et al., 2007; Donahue et al., 2009).

– Volatile organic compounds (VOC, $C^* > 3\times10^6$ μg m^{-3}). These compounds do not partition into the particles. They can be important SOA precursors.

From a wide prospective, almost all organic compounds associated with the condensed phase may be considered as semi-volatile. They can be found both in gas phase and particle phase with different fractions respective of their volatility. The partitioning coefficient (ξ), the fraction of a given compound observed in condensed phase, is very helpful in determining the contribution of these organic compounds to SOA formation. Donahue at al. demonstrated that the partitioning coefficient (ξ) is dependent on the saturation concentration (C^*) and the total organic aerosol mass concentration, as shown in the following equation. The partitioning coefficient is dynamic with respect to different OA loading and different temperature, which changes the saturation concentration (Donahue et al., 2006).

$$\xi_i = \left(1 + \frac{C_i^*}{C_{OA}}\right)^{-1}; C_{OA} = \sum_i C_i \xi_i$$

For example, if C_{OA} = 10 μg m^{-3} and a given compound has C_i^* = 10 μg m^{-3}, the partitioning coefficient (ξ) will be 0.5. We would expect half of the mass of that compound in the condensed

phase and half in the vapor phase. When C_i* < 10 μg m^{-3}, more than 50% of that compound will stay in the particle phase. When SOA loading is increased to 100 μg m^{-3}, the ξ of the compound with C_i* = 10 μg m^{-3} becomes 0.9. At this time, 90% of that compound should be observed in the condensed phase.

Following the partitioning theory, the volatility distribution of all organic compounds in the particle phase and gas phase can be demonstrated in the volatility basis set (VBS) (Donahue et al., 2006). The VBS consists of a group of lumped compounds with fixed C* values, comprising up to 9 "bins" separated by one order of magnitude each in C^* at 300K. Using the VBS, the products with different volatilities from SOA-forming reactions can be mapped over the range of organic aerosol mass concentration while maintaining mass balance for more volatile co-products. Along with volatility, the carbon oxidation state is another important factor during the oxidation of organic compounds. The 2-D VBS was developed with two coordinates, the volatility (C^*) and the average carbon oxidation state (OS_C) (Donahue et al., 2012b;Donahue et al., 2009). The 2-D VBS reasonably constrains average organic aerosol composition in the atmosphere based on only these two measurable organic properties.

1.4 Ageing and Mixing

SOA formation in the atmosphere is a dynamic process, both physically and chemically. For the semi-volatile organics, mass is constantly shifting between the aerosol and gas phases. Due to continuous VOC and aerosol emissions, and the effect of oxidants, the composition and properties of SOA may change continuously. In some circumstances, the further evolution of organic aerosols may be more important than the initial formation. Chemical ageing and mixing are two important processes during the evolution of organic aerosols.

Chemical ageing is the further reaction of first-generation oxidation products with OH radicals, which makes the SOA vapors further oxygenated and less volatile (Henry and Donahue, 2012;Donahue et al., 2012a). This will absolutely increase the organic aerosol mass and alter the properties of aerosols. Heterogeneous oxidation is almost certainly a factor of 5–20 slower than the corresponding homogeneous oxidation due to diffusion limitations. So the oxidation of the SOA vapors dominates the chemical ageing process. VOCs and organic aerosols emitted from different sources usually have different chemical compositions. The SVOCs may cross-partition between different types of organic aerosols based on their characteristics (Robinson et al., 2013;Hildebrandt et al., 2011). The mixing process increases the complexity of organic aerosols by adding different organic species and increases the chances of chemical reaction inside the aerosols.

1.5 SOA formation in the CMU smog chamber

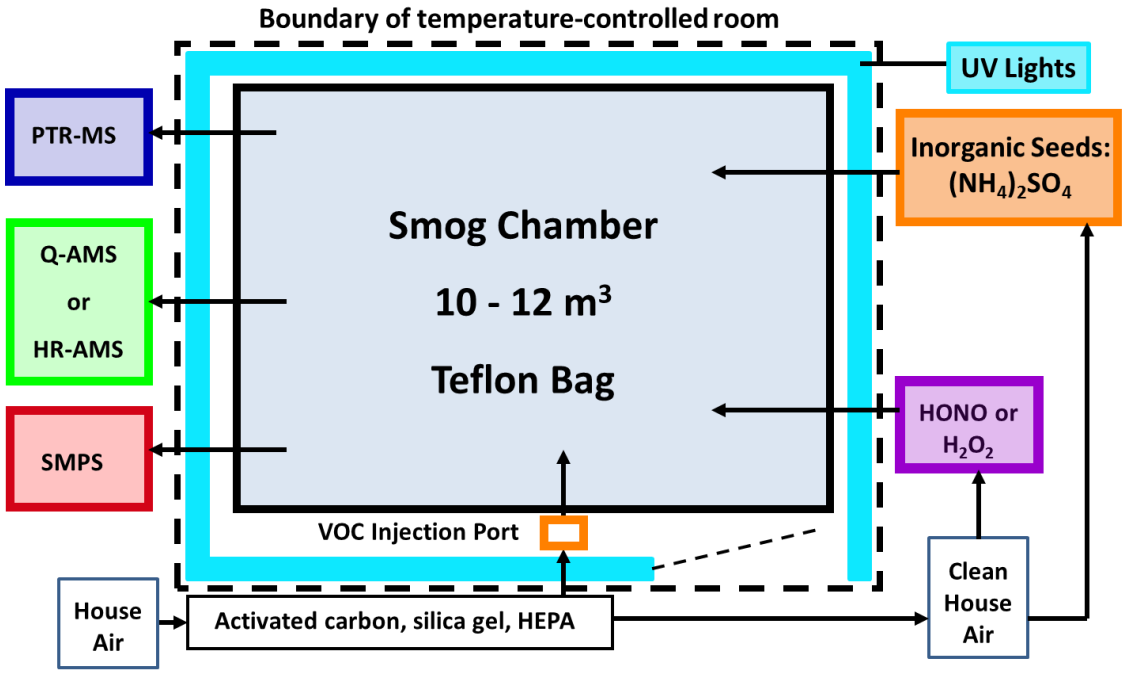

Scheme 1.1 Smog chamber of the Center for Atmospheric Particle Studies (CAPS) at CMU

Batch experiments were conducted in the smog chamber of the Center for Atmospheric Particle Studies (CAPS) at CMU. Figure 1 shows the set-up of the smog chamber. Many details of the experimental procedures are described in (Hildebrandt et al., 2009). The chamber is a 10 m^3 Teflon bag (Welch Fluorocarbon) suspended inside a temperature controlled room. The temperature was set at 295K. Before each experiment, the bag was cleaned under the UV light, with dry, clean air created by passing compressed air through high-efficiency particulate air (HEPA) filters and activated-carbon filters to remove particles and organic vapors, and through silica gel to remove moisture. For each experiment, hydrogen peroxide (H_2O_2) or nitrous acid (HONO) was then introduced into the chamber by bubbling clean, heated air through a water solution. Ammonium sulfate ($(NH_4)_2SO_4$, Sigma Aldrich, 99.99%) seed particles were created using a constant-output atomizer (TSI, model 3075) and were passed through a diffusion dryer and a neutralizer into the chamber. Nitric oxide (NO) was added to the chamber for high-NO_x (=$NO+NO_2$) experiments using a high-pressure gas cylinder of 0.01% NO in N_2 (Valley National Gas). VOCs were added via a septum through which clean air passed to vaporize the terpene and carry it into the chamber. SVOCs were introduced to the chamber via a flash vaporizer in which the organic compound was rapidly heated on the tip and transferred to the chamber. The walls of the temperature-controlled room are lined with UV lights (General Electric model 10526 black). After the particles and gases were injected into the chamber and allowed to mix, the UV lights were turned on to generate OH radicals and initiate photo-oxidation reactions and SOA formation.

Particle number and volume inside of the chamber were measured using a scanning mobility particle sizer (SMPS, TSI classifier model 3080, CPC model 3071 or 3010). Particle mass was also measured directly by a High Resolution Aerosol Mass Spectrometer (HR-AMS, Aerodyne

Research, Inc.). Concentrations of VOCs were measured by Gas Chromatography–Mass Spectrometry (GC-MS) or by Proton Transfer Reaction Mass Spectrometry (PTRMS). Ozone and NOx concentrations were measured by gas-phase analyzers (Dasibi model 1008-PC, Teledyne model 200EU). Temperature and relative humidity were measured using thermistors and a commercial humidity sensor.

1.6 SOA mass yield and wall loss correction

The SOA mass yield from a reaction is defined as the mass of organic aerosol formed divided by the mass of precursor consumed (Odum et al., 1996).

$$Y = \frac{C_{OA}}{\Delta C_{precursor}}$$

Where C_{OA} is the mass of organic aerosol formed, and $\Delta C_{precursor}$ is the mass of the precursor organic species consumed to form the organic aerosol (C_{OA}) and other products.

We determined SOA mass yields for PD with the aid of inorganic seeds, ammonium sulfate, which promote condensation and allow an independent measurement of particle wall losses. We injected dried ammonium sulfate particles up to ~20 to 25 μg m^{-3}. The ammonium sulfate concentration is inside the range of a typical ambient aerosol mass concentration of between 5 and 30 μg m^{-3} (Kanakidou et al., 2005).

To obtain the total $C_{OA}(t)$ from the suspended mass concentration, we correct for wall losses, assuming that organic particles lost to the wall are in equilibrium with the suspended particles and vapor-phase species. Total SOA production (C_{OA}) is determined by using the ratio of suspended organic aerosol (C_{OA}^{sus}) to suspended ammonium sulfate (C_{seed}^{sus}) and the initial

concentration of ammonium sulfate C_{seed}^{sus} $(t = 0)$, as described in the literature (Hildebrandt et al., 2009):

$$C_{OA}(t) = \frac{C_{OA}^{sus}(t)}{C_{seed}^{sus}(t)}\ C_{seed}^{sus}(t = 0)$$

$C_{seed}^{sus}(t)$ can be obtained by fitting an exponential decay to the ammonium sulfate volume concentration (measured with the SMPS) over the interval between seed injection (and mixing) in the chamber and the onset of photo-oxidation. Extrapolation of this signal after the photo-oxidation process starts defines the seed mass concentration as a function of time. At time 0 (onset of photo oxidation) and later, the difference between the total aerosol mass concentration in the chamber (measured with an SMPS) and the extrapolated ammonium-sulfate mass concentration is considered as $C_{OA}^{sus}(t)$. The ratio of C_{OA}^{sus} to C_{seed}^{sus} can also be measured by HR-AMS, which is equal to the ratio of organic to seeds (ammonium and sulfate) concentration in the suspended particles.

1.7 Overview of the studies included in the thesis.

As showed in figure 2, SVOC vapors plays a very important role during SOA formation, mixing, ageing and other evolution of SOA. This thesis focused on studying the SOA formation from an SVOC (pinanediol), the interaction between the SVOCs vapor and Teflon chamber wall, and the sorption of SVOC vapors into PEG seeds.

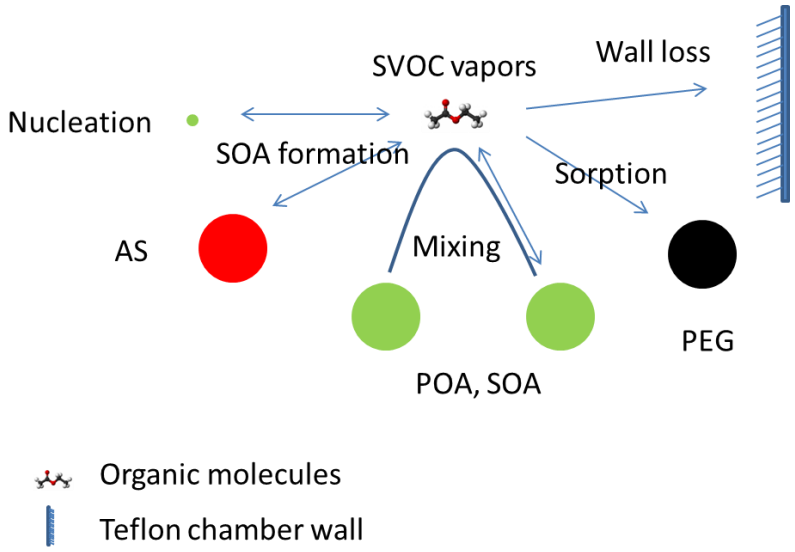

Scheme 1.2 Mass transfer between the particle phase, gas phase and Teflon chamber wall during the SOA formation, mixing, sorption and wall loss process.

In Chapter 2, we study the SOA formation from PD with HONO as the OH radical source. The wall deposition of PD was explored by comparing the total amount of PD added into the chamber and the real PD concentration in the gas phase, which was measured with GERSTEL thermal desorption gas chromatography. We also investigated the release of PD on the chamber wall by diluting or heating up the chamber. We analyzed SOA mass yield of PD and the elemental composition of the formed SOA. The wall loss of PD was corrected. The distribution of volatility and oxidized state of the organic products were presented in the two-dimensional volatility-oxidation space. The results in this study are comparable with what was observed in CLOUD.

In Chapter 3, we investigate the vapor wall loss based on the change of SVOC concentrations on the particles. Ammonium sulfate (AS) was used as seed to constrain the particle wall loss. Then we could separate the mass loss of SVOCs due to vapor wall loss and particle wall loss. Through model simulations of gas-particle-wall partitioning of SVOCs, we calculated the vapor wall loss

rate. The results clearly show that the vapor wall loss rate of SVOCs is consistently proportional to the vapor concentrations of SVOCs in the gas phase.

In Chapter 4, we describe experimental techniques for performing the sorption of semi-volatile α-pinene SOA into non-volatile PEG seeds and demonstrate the use of HR-AMS in determining the mass of SOA in a mixture of SOA and PEG. We verified that PEG was a robust seed to study the SOA properties and formation even with oxidants present. We figure out that the PEG could be separated with α-pinene SOA based on their unique fragments on the mass spectra measured by the AMS. We observed the uptake of α-pinene SOA vapors into PEG and compared the difference between α-pinene SOA formed with HONO and O_3 under the different SOA loadings.

1.8 Reference

Atkinson, R., and Arey, J.: Atmospheric Degradation of Volatile Organic Compounds, Chemical Reviews, 103, 4605-4638, 2003.

Barsanti, K. C., and Pankow, J. F.: Thermodynamics of the formation of atmospheric organic particulate matter by accretion reactions—Part 3: Carboxylic and dicarboxylic acids, Atmospheric Environment, 40, 6676-6686, 2006.

Donahue, N. M., Robinson, A. L., Stanier, C. O., and Pandis, S. N.: Coupled partitioning, dilution, and chemical aging of semivolatile organics, Environmental Science & Technology, 40, 2635-2643, 2006.

Donahue, N. M., Robinson, A. L., and Pandis, S. N.: Atmospheric organic particulate matter: From smoke to secondary organic aerosol, Atmospheric Environment, 43, 94-106, 2009.

Donahue, N. M., Henry, K. M., Mentel, T. F., Kiendler-Scharr, A., Spindler, C., Bohn, B., Brauers, T., Dorn, H. P., Fuchs, H., Tillmann, R., Wahner, A., Saathoff, H., Naumann, K.-H., Möhler, O., Leisner, T., Müller, L., Reinnig, M.-C., Hoffmann, T., Salo, K., Hallquist, M., Frosch, M., Bilde, M., Tritscher, T., Barmet, P., Praplan, A. P., DeCarlo, P. F., Dommen, J., Prévôt, A. S. H., and Baltensperger, U.: Aging of biogenic secondary organic aerosol via gas-phase OH radical reactions, PNAS, 109, 13503-13508, 2012a.

Donahue, N. M., Kroll, J. H., Pandis, S. N., and Robinson, A. L.: A two-dimensional volatility basis set – Part 2: Diagnostics of organic-aerosol evolution, Atmos. Chem. Phys., 12, 615-634, 2012b.

Goldstein, A. H., and Galbally, I. E.: Known and Unexplored Organic Constituents in the Earth's Atmosphere, Environmental Science & Technology, 41, 1514-1521, 2007.

Hallquist, M., Wenger, J. C., Baltensperger, U., Rudich, Y., Simpson, D., Claeys, M., Dommen, J., Donahue, N. M., George, C., Goldstein, A. H., Hamilton, J. F., Herrmann, H., Hoffmann, T., Iinuma, Y., Jang, M., Jenkin, M. E., Jimenez, J. L., Kiendler-Scharr, A., Maenhaut, W., McFiggans, G., Mentel, T. F., Monod, A., Prévôt, A. S. H., Seinfeld, J. H., Surratt, J. D., Szmigielski, R., and Wildt, J.: The formation, properties and impact of secondary organic aerosol: current and emerging issues, Atmos. Chem. Phys., 9, 5155-5236, 2009.

Henry, K. M., and Donahue, N. M.: Photochemical aging of α-pinene secondary organic aerosol: Effects of OH radical sources and photolysis, The Journal of Physical Chemistry A, 2012.

Hildebrandt, L., Donahue, N. M., and Pandis, S. N.: High formation of secondary organic aerosol from the photo-oxidation of toluene, Atmos. Chem. Phys., 9, 2973-2986, 2009.

Hildebrandt, L., Henry, K. M., Kroll, J. H., Worsnop, D. R., Pandis, S. N., and Donahue, N. M.: Evaluating the mixing of organic aerosol components using high-resolution aerosol mass spectrometry, Environmental Science & Technology, 45, 6329–6335, 2011.

Kroll, J. H., and Seinfeld, J. H.: Chemistry of secondary organic aerosol: Formation and evolution of low-volatility organics in the atmosphere, Atmospheric Environment, 42, 3593-3624, 2008.

Oberdörster, G., Sharp, Z., Atudorei, V., Elder, A., Gelein, R., Kreyling, W., and Cox, C.: Translocation of Inhaled Ultrafine Particles to the Brain, Inhalation Toxicology, 16, 437-445, 2004.

Odum, J. R., Hoffmann, T., Bowman, F., Collins, D., Flagan, R. C., and Seinfeld, J. H.: Gas/particle partitioning and secondary organic aerosol yields, Environ. Sci. Technol., 30, 2580-2585, 1996.

Pope, C. A., and Dockery, D. W.: Health Effects of Fine Particulate Air Pollution: Lines that Connect, J Air Waste Manage, 56, 709-742, 2006.

Pope, C. A., Ezzati, M., and Dockery, D. W.: Fine-Particulate Air Pollution and Life Expectancy in the United States, New England Journal of Medicine, 360, 376-386, 2009.

Robinson, E. S., Saleh, R., and Donahue, N. M.: Organic aerosol mixing observed by single-particle mass spectrometry, The Journal of Physical Chemistry A, 117, 13935-13945, 2013.

Seinfeld, J. H., and Pankow, J. F.: ORGANIC ATMOSPHERIC PARTICULATE MATERIAL, Annual Review of Physical Chemistry, 54, 121-140, 2003.

Solomon, S. Q., D.; Manning, M.; Alley, R. B.; Berntsen, T.; Bindoff, N. L.; Chen, Z.; Chidthaisong, A.; Gregory, J. M.; Hegerl, G. C.: Climate change 2007: The physical science basis, contribution of working group 1 to the fourth assessment report of the Intergovernmental Panel on Climate Change, 2007.

Chapter 2

Secondary organic aerosol production from pinanediol

Abstract

We have investigated the production of secondary organic aerosol (SOA) from pinanediol (PD), a precursor chosen as a surrogate for first-generation oxidation products of monoterpenes. Monoterpenes have substantial emissions from vegetation, and when they are oxidized some products have very low vapor pressure and thus contribute to SOA formation. Experiments at the CLOUD facility at CERN are focusing on chemistry that can drive formation of new particles in the atmosphere (nucleation), and further oxidation of products such as PD has been proposed as an important contributor to nucleation. We focus on tracking the chemical composition change and SOA formation from PD in the CMU smog chamber. We observed that PD showed a large chamber wall deposition and reached a steady concentration. Only around 14% of PD was left in the gas phase. When increasing chamber temperature from 13 to 44 ^{o}C 3 times increase in PD vapor concentration indicated the release of PD from the chamber walls. But we did not observe the release of PD from the chamber walls during isothermal dilution of the chamber with fresh air at 22 ^{o}C, which simulated the decrease of PD concentration in the gas phase due to the chemical reaction with OH radicals. So we considered the release of PD from the chamber walls was negligible under the experimental conditions in this study. SOA mass yields were observed at 0.1~1, which were around 2 or 3 times larger than monoterpenes. The average carbon oxidation states were calculated as around -0.7,

which were similar to the value observed in CLOUD. We also studied the distribution of volatility and oxidized state of the organic products in the two-dimensional volatility-oxidation space. Our data are consistent with ~10% of the SOA with low volatility that could drive new particle formation.

2.1 Introduction

Particulate matter (PM) in the atmosphere has shown important impacts on human health and life expectancy (Pope et al., 2009) and also influences on Earth's climate by absorbing and scattering radiation (Solomon, 2007). Organic compounds constitute a large fraction of particulate matter (PM) in the atmosphere. They make up around 20–90% of the aerosol mass in the lower troposphere (Kanakidou et al., 2005). Secondary organic aerosol (SOA), formed from oxidation of organic materials in atmosphere, accounts for a significant fraction of the organic mass in PM (Zhang et al., 2007). The oxidation of organic material in the atmosphere is dynamic due to constant photo-oxidation and associated evolution in thermodynamic properties (Seinfeld and Pandis, 2006). Further oxidation of the products from SOA formation may add more functional groups, such that the "second-generation" oxidation may be even less volatile and more water soluble, and also enhance the SOA mass (Donahue et al., 2012;Henry and Donahue, 2012). Here we used pinanediol (PD) as a surrogate for first-generation oxidation products of monoterpenes to study this ageing chemistry.

Particles are the nuclei for cloud droplets. The Cosmics Leaving OUtdoor Droplets (CLOUD) facility at CERN is designed to study the effects of cosmic rays on new particle formation (nucleation and growth) involving sulfuric acid vapor and different

stabilizing species (Kirkby et al., 2011;Schobesberger et al., 2013;Riccobono et al., 2014). These stabilizing species include the ammonia, organic amines as well as oxidation products of organic precursors. PD was used to mimic first-generation oxidation products of monoterpene formed in the atmosphere (Schobesberger et al., 2013). Specifically the experiments addressed the hypothesis that oxidation of these first generation products by OH radicals can produce later generation products with sufficient supersaturation to participate in nucleation (Donahue et al., 2011b). The experiments confirmed that highly oxidized organic compounds can play a direct role in the very first steps of the formation nanoparticles (clusters) and their growth between 1 and 2 nm. Experiments are among the first to observe highly oxidized extraordinary low volatile organic compounds (ELVOC) (Donahue et al., 2011a), which retained 10 carbon atoms with 2-12 oxygen atoms. The composition of these remarkably highly oxidized organic compounds and possible mechanisms for their formation has attracted much attention in this research field (Ehn et al., 2014).

In this research, we focused on studying the SOA formation from PD using HONO photolysis as an OH source in CMU chamber. We explored the wall deposition of PD by comparing the total amount of PD added into the chamber and the observed PD concentration in the gas phase. We also investigated the release of PD from the chamber walls by diluting or heating up the chamber. We then calculated the SOA mass yield and the elemental composition of the formed SOA accounting for the loss of PD. We analyzed the distribution of volatility and oxidized state of the organic products in the two-dimensional volatility-oxidation space (2D-VBS) and compared the properties of bulk SOA to the ELVOC observed in CLOUD.

2.2 Materials and methods

Batch experiments were conducted in the smog chamber of the Center for Atmospheric Particle Studies (CAPS) at CMU. Many details of the experimental procedures were described in a previous paper (Hildebrandt et al., 2009). Only a brief description is provided here. The chamber is a 10-m^{-3} Teflon bag (Welch Fluorocarbon) suspended inside a temperature controlled room. The temperature was maintained at 22 ^{o}C for the SOA formation experiments. Before each experiment, the chamber was cleaned under the UV light with dry, clean air created by passing compressed air through high-efficiency particulate air (HEPA) filters and activated-carbon filters to remove particles and organic vapors, and through silica gel to remove moisture. Ammonium sulfate ($(NH_4)_2SO_4$, Sigma Aldrich, 99.99%) seed particles were created from a 1g L^{-1} aqueous solution using a constant-output atomizer (TSI, model 3075) to form droplets that passed through a diffusion dryer and a neutralizer into the chamber. HONO was added to the chamber by bubbling filtered air through a nitrous acid solution for 20 min. *n*-tridecane, 1-tridecene, 2-nonanone, 2-Nonanol, PD (Sigma-Aldrich, 99%) and oxy pinocamphone (OPC, Sigma-Aldrich, 99%) was introduced to the chamber via a flash vaporizer. A small, resistive metal heater enclosed in a stainless steel sheath was used to flash the organic material into the chamber. The organic material was placed on the stainless steel surface before the heater was inserted into the chamber on the end of a long tube. With a flow of clean, dry dispersion air used to mix the chamber, the heater was power-cycled until there was no increase in organic concentrations. UV lights (General Electric model 10526 black) are lined on the walls of the temperature-controlled room. After the seeds and precursors

were injected into the chamber and allowed to mix, the UV lights were turned on to generate OH radicals and initiate photo-oxidation reactions and SOA formation.

Suspended particle number and volume were measured using a scanning mobility particle sizer (SMPS, TSI classifier model 3080, CPC model 3071 or 3010). In order to convert the SMPS volume measurements to mass concentrations, an organic mass density of 1.3 g cm^{-3} was used, which was calculated following the method in the literature (Nakao et al., 2013). Particle mass concentrations were also measured directly by a high resolution aerosol mass spectrometer (HR-AMS, Aerodyne Research, Inc.). The concentrations of PD in the gas phase were measured by proton transfer reaction mass spectrometry (PTRMS, Ionicon Analytik). The temperature of the inlet line was maintained at 60 ^{o}C. The concentration of organic species in the gas phase were analyzed by a gas chromatograph/mass spectrometer (GC/MS) (Agilent, 6890 GC/5975 MS) equipped with a thermal extraction and injection system (TDGC/MS, Gerstel) and a capillary column (Agilent HP-5MS, 30 m × 0.25 mm) (Zhao et al., 2014). The samples were collected by sampling chamber air through Tenax® TA filled glass tubes (Gerstel 6mm OD, 4.5mm ID glass tube filled with ~290 mg of Tenax TA) at a flow rate of 0.5 L/min for 2 minutes. The recovery of organics during analysis was tracked using deuterated standards that were spiked into each Tenax tube prior to the thermal desorption. Ozone and NO_x concentrations were measured by gas-phase analyzers (Dasibi model 1008-PC, Teledyne model 200EU). Temperature and relative humidity were measured using thermistors and a commercial humidity sensor.

2.3 Results and Discussion

2.3.1 Correction of loss of pinanediol vapor to the chamber wall.

Matsunaga and Ziemann showed that organic vapors can sorb reversibly into Teflon chamber walls (Matsunaga and Ziemann, 2010). Volatile organic compounds (VOCs) may partition to the chamber walls and cause the concentration in the gas phase lower than the expected value. Relatively volatile organics appear to partition reversibly onto the Teflon. The fraction of organic vapors left in gas phase is mostly determined by the volatility of the organics, and also the organic molecule structure. The reversible partitioning can be parameterized by treating the Teflon wall as a sorptive medium with an effective mass of 2-24 mg m^{-3} (Matsunaga and Ziemann, 2010). 2-decanol ($C_{10}H_{21}OH$) showed significate vapor loss. The extra OH group decreases the C^o of PD by about 2.3 decades, which results in larger fraction of PD loss to the chamber walls. In order to get the accurate SOA mass Yield of PD, the loss of PD vapor needs to be determined. We selected *n*-tridecane, 1-tridecene, 2-nonanone, 2-Nonanol and two SOA precursor, oxy pinocamphone and PD to measure the vapor wall loss. We injected a series of aliquot into the chamber in increments of 11 ppbv (at 100% injection efficiency). We used PTRMS to trace the organic vapor concentrations in the chamber. Organics were also collected with Tenax tubes and analyzed by TDGC/MS.

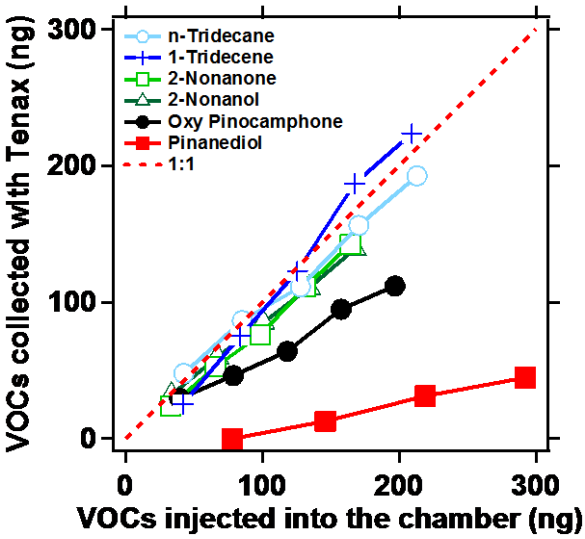

Figure 2.1 The concentration of *n*-tridecane, 1-tridecene, 2-nonanone, 2-Nonanol, oxy pinocamphone and pinanediol measured by thermal desorption gas chromatography (GERSTEL).

Figure 2.1 compares the amount of all six VOC vapors in the gas phase with the injected amount. The amount of *n*-tridecane, 1-tridecene, 2-nonanone and 2-Nonanol in the gas phase in the chamber and their injected amount lines up along the 1:1 line, demonstrating almost no wall losses for these compounds. Our observations are consistent with Matzunaga and Ziemann's results. However, large discrepancies were observed between the collected and injected amounts for PD and OPC. Abound 34% of OPC was lost to the chamber wall. Only around 14% of PD stayed in the gas phase; 86% was lost to the chamber wall. The significant loss of precursor needs to be measured and accounted for when studying the SOA formation from SVOCs in Teflon chamber.

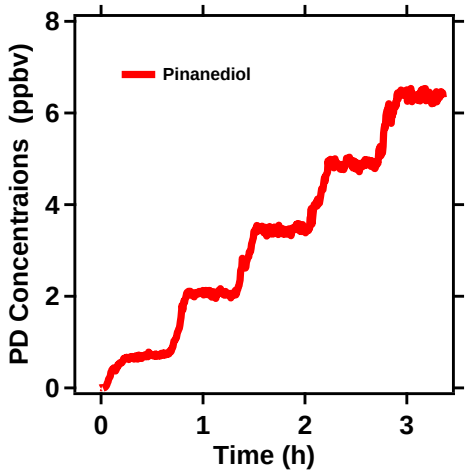

Figure 2.2 Gas phase concentration of pinanediol measured by PTR-MS.

Figure 2.2 shows that the temporal change of PD vapor concentrations measured by The PTR-MS. A fragment (*m/z*=135, $C_{10}H_{15}^{+}$) was used to track vapor concentrations of PD. The PD vapor concentrations measured by PTR-MS were calculated by comparing the signal of m/z 135 with measurements of TDGC/MS. The results showed the vapor concentrations of PD stabilized rapidly after each injection. Each injection with same amount of PD resulted in a similar vapor concentration increase, indicating that the wall loss factor of PD was almost constant in this concentration range.

In order to test the reversibility of sorption of PD, we used heating and isothermal dilution of the chamber. We put a fairly large amount of PD into the chamber. As shown in figure 2.3, the concentration was 866μg m^{-3} (118ppbv) after the injection. After that, we increased the chamber temperature (red) from 13 ^{o}C to 44 ^{o}C at time 0h. The PD vapor concentration measured by PTRMS (green) increased rapidly and reached a steady value after the temperature reached 44 ^{o}C. The concentration was around 3 times larger than the initial concentration. To confirm that PD was coming from the chamber walls,

we also measured the particle concentration with HR-AMS (blue). The total organics in particles was around 5 μg m^{-3}, far less than the increase of the PD vapor concentration in the gas phase; Particles were not the dominant source for this extra PD. The only possible source was the PD adsorbed or absorbed by the Teflon chamber walls.

Increasing temperature by 30 ^{o}C should increase the saturation concentration (C^{*}) of PD by roughly a factor of 30. All else being equal, this should cause a 30 fold increase in the activity of the PD in the Teflon and thus drive a large return flux to the gas phase, with the equilibrium vapor fraction increasing from 10% to around 80%. This is consistent with our observations though we observe a factor of 2-3 less than this simple calculation would suggest. The next question is how quickly PD on the chamber walls goes into the gas phase under the experimental conditions in SOA formation experiments at 22 ^{o}C.

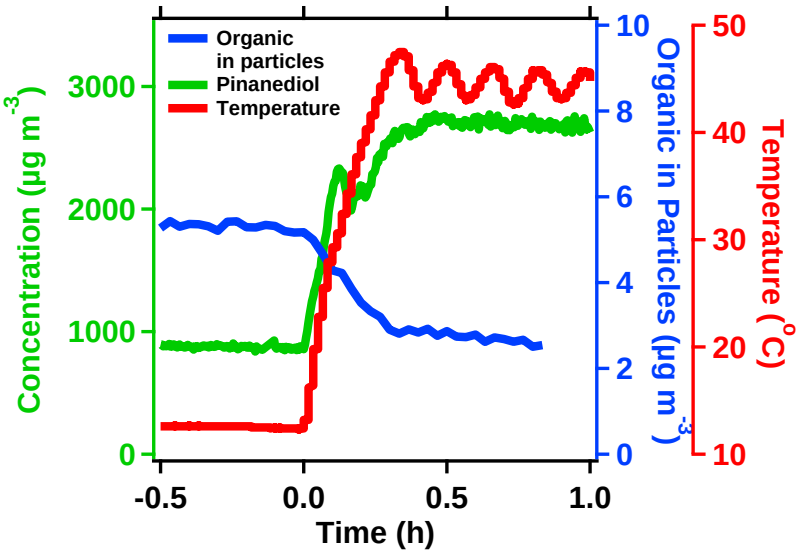

Figure 2.3 Vapor concentration increase of pinanediol after increasing the chamber temperature from 13 ^{o}C to 44 ^{o}C. The concentrations of pinanediol (green) are shown on the left. Temperature is shown on the right as red. The organic concentrations in the particles are shown as blue on the right.

To examine the release of PD from Teflon chamber walls during isothermal SOA formation, we used dilution to simulate the PD concentration decrease due to the chemical reaction with OH radicals. After injecting PD, we flushed the chamber continuously with fresh air with the chamber open to atmosphere. Acetonitrile (AN), which does not have wall losses, was injected along with PD to track the dilution. Figure 2.4 shows the change of concentrations of PD and AN during the dilution. The ratio of PD to AN will be constant if there is no PD released from the Teflon chamber wall. Dilution started at time 0h with 100 Lpm (1% min^{-1} of the chamber volume) fresh air flow. The concentrations of both PD and acetonitrile steadily decreased. However, the ratio of PD to acetonitrile (blue) was almost constant. This indicated that PD was still being lost to the chamber walls, though only slightly. To achieve a large dilution rate, we increased fresh air flow to 300Lpm (3% min^{-1}) at 3.5h while the PD concentration dropped to 30µg m^{-3}, around 30% of the initial concentration. We still did not observe any PD released from the wall. Only after the PD concentration reached 2 µg m^{-3} at 5.5h, which is only 2% of the initial concentration, did the ratio of PD to acetonitrile (blue) begin to increase, indicating that PD came back to the gas phase from the chamber walls. PD concentration (green) also showed a clear curving up after 5.5h. The observation clearly shows that the change of PD concentration due to the interaction with the chamber walls (deposition and releasing) during SOA formation was very small and negligible under the experimental conditions.

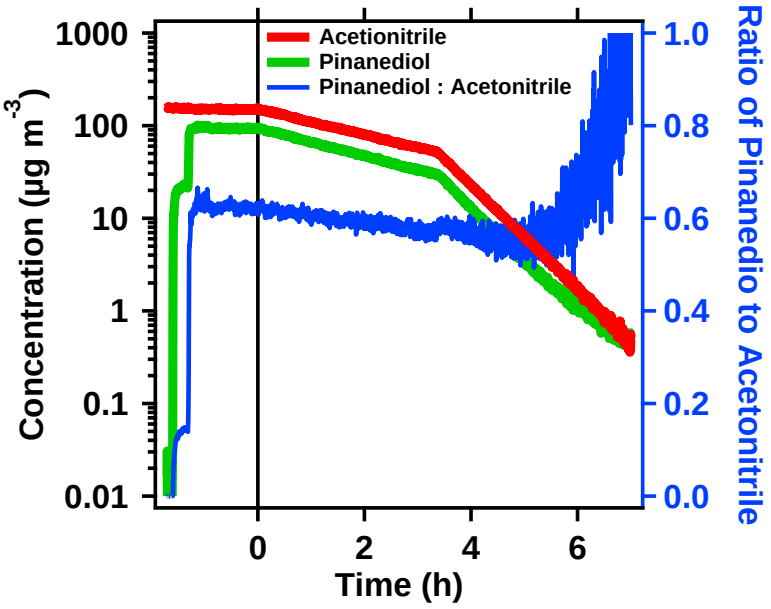

Figure 2.4 Vapor concentration change of pinanediol (green) and acetonitrile (red) during diluting the chamber with fresh air. The blue line showed the ratio of pinanediol to acetonitrile.

Our overall findings show clear evidence that PD is lost to the chamber walls, with a constant fraction of about 14% remaining in the gas phase at 22°C. Heating by 30°C released a fraction of the trapped PD but not all of it and less than what would be expected from purely reversible partitioning. Furthermore, isothermal dilution that mimicked the loss of PD via oxidation showed no sign of PD returning to the gas phase, indicated by a constant PD to acetonitrile ratio measured via PTRMS. Thus, while reversible partitioning to the walls is the most straightforward explanation for the losses of PD, we see no sign of reversibility under the conditions of our SOA formation experiments. It is therefore reasonable to assume that the measured concentration by the PTRMS can be calibrated by the measurements with TD-GCMS and consequently the decrease in the observed PD concentration by PTRMS would represent the actual change of gas-phase PD concentrations during the experiments. However, as a precaution against

return flux after substantial PD depletion, we shall limit our analysis to the first 1.5 e-folding lifetimes in PD oxidation (we ignore all data where the PD concentration is less than 22% of its initial value).

2.3.2 Oxidation of PD by OH radicals.

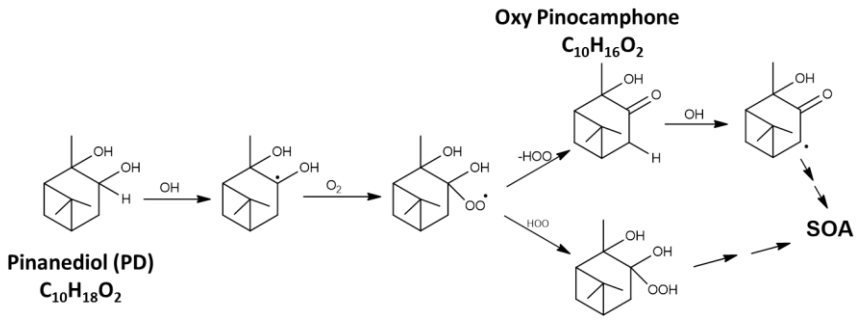

Scheme 2.1 The proposed mechanism of the oxidation of pinanediol by OH radicals.

The first two important steps of the oxidation of PD by OH radicals are hydrogen atom abstraction and addition of O_2 (Seinfeld and Pankow, 2003). With high reactivity, OH radicle easily grabs a hydrogen atom from organic molecules and leaves an alkyl radicals ($R\cdot$). The most active hydrogen atom in PD is the α-H, as show in scheme 2.1. Due to abundant O_2 in the atmosphere (21%), the lifetime of alkyl radicals is very short. They will react with O_2 very quickly and form relatively stable species, peroxide radicles ($ROO\cdot$). The PD peroxide radicles may eliminate $HOO\cdot$ and produce oxy pinocampone; or get another hydrogen atom and become hydroperoxide. The oxy pinocamphone and the hydroperoxide may undergo further oxidation and produce low volatile products to partition into suspended particles and form SOA.

2.3.3 The concentrations of particles and PD vapor during SOA formation

Three instruments using to monitor the concentrations of particles and organic vapor during experiments, are SMPS, HR-AMS and PTR-MS. Figure 2.5-2.7 shows the results from these three instruments for the SOA formation of PD using HONO photolysis as an OH source. The PTRMS was used to trace the PD vapor concentration by measuring the fragment of PD, *m/z*=135. As shown in figure 2.5, after the UV lights were turned on at time 0h, the PD concentration began to decrease due to the chemical reaction with OH radicals. Around 80% of PD were reacted in 1 hour. The gray part, where the PD concentration was less than 22% of its initial value, was not used when calculating the SOA mass yields. We calcualted how much PD reacted to obtain $\Delta C_{precursor}$ in equation 2.1 for calculating the SOA mass yield (Y).

$$Y = \frac{C_{OA}}{\Delta C_{precursor}} \qquad (2.1)$$

where C_{OA} is the mass of organic aerosol created, and $\Delta C_{precursor}$ is the mass of the precursor organic species consumed to form the organic aerosol (C_{OA}) and other products.

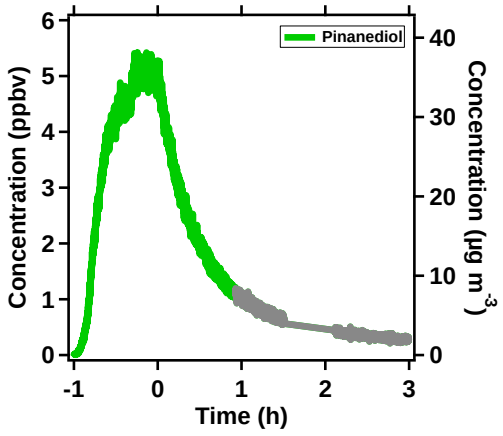

Figure 2.5 Vapor concentration change of pinanediol (PD) measured from PTR-MS during the SOA formation experiment from PD. The gray part (less than 22% of its initial value) was not used when calculating the SOA mass yields.

The condensation sink (CS) is the loss freqence of vapors to the aerosol surface, it can be thought of as the mean speed of the vapors multiplied by the aerosol surface area, but modified for gas phase diffusion near the particl surface. We calculated the CS^P using equation 2.2 (Trump et al., 2014).

$$CS^P = \sum_k N_k \frac{v}{4} \pi D_{P,k} \beta_k$$

(2.2)

where *k* refers to a particle size bin, N_k is the number concentration of particles in this bin, v is the mean thermal speed of the gas phase molecules, $D_{P,k}$ is the particle diameter, and β is the transition regime correction factor (Seinfeld and Pandis, 2006).

Figure 2.6 shows particles distribution from the SMPS. The red curves are the 20 minuntes average results just before the SOA formation. The blue curves show the 20 minuntes average results from 35 to 55 mins after SOA formation started. All three distruibution (bottom) shifted to larger particle region after the SOA formation because the condensation of lower volatility vapors grew the particles bigger. The mass (top) concentrations were calculated base on the particle volumes with unit particle density. Larger partilces contribute to more surface aea and even more volume. So the observed peak of the condensation sink distribuion was larger than the peak of the number distribution. The peak of the mass distrubtion of suspends particles was larger that both of them.

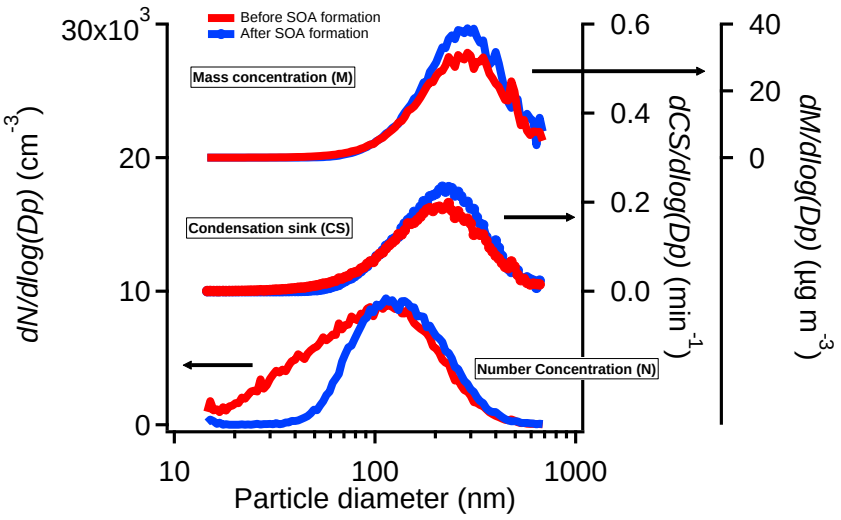

Figure 2.6 Mass (top), condensation sink (middle) and number distribution (bottom) of particles measured or calculated from SMPS in 20 minutes average before and 35 to 55 mins after the SOA formation experiment from PD.

Figure 2.7 shows the total mass concentration (green), condensation sink (blue) and number concentration (red) of the particles. Before time 0h, there were only ammonium sulfate seeds in the chamber. The decrease in condensation sink, mass and number concentration was due to continuous particle losses to the chamber walls. At time 0h, chemical reaction of PD with OH radicals was initiated and oxidation products formed from PD, with lower volatility, condensed on the AS seeds and made the particles grow. The growth of particles was faster than the mass wall loss of particles, so we observed an increase in total suspended particle mass and condensation sink. After 1 hour, when around 80% of the PD had reacted, the formation of SOA became smalller than the mass wall loss of particles. The condensation sink and mass contration of particles thus turned to decrease. The continuous decrease of number concentration of the particles indicated there was no new particle formation.

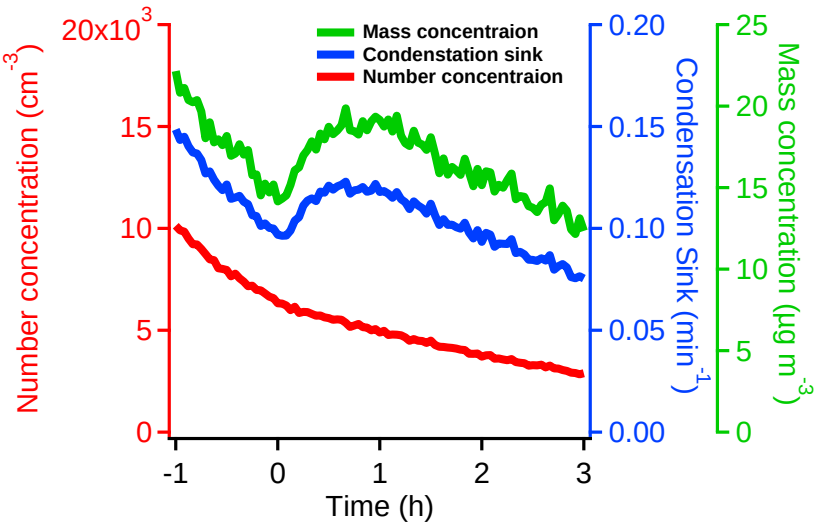

Figure 2.7 Mass concentration, condensation sink and number concentration of particles measured or calculated from SMPS during the SOA formation experiment from PD.

The loss of the particle mass to the chamber walls needs to be accounted for in order to get the total amount of formed SOA, The corrected SOA production (C_{OA}) is determined by using the ratio of suspended organic aerosol (C_{OA}^{sus}) to suspended ammonium sulfate (C_{seed}^{sus}) and the initial concentration of ammonium sulfate C_{seed}^{sus} $(t = 0)$ at time 0h, as described in the literature (Hildebrandt et al., 2009):

$$C_{OA}(t) = \frac{C_{OA}^{sus}(t)}{C_{seed}^{sus}(t)} C_{seed}^{sus}(t = 0) \qquad (2.3)$$

As shown in figure 2.8, $C_{seed}^{sus}(t)$ was obtained by fitting an exponential decay to the bare ammonium sulfate concentrations in one hour before photo oxidation started, then extrapolating it over the whole SOA formation period (black). Considering the coagulation of particles is very small, as low as 1%, so the decrease of particle number concentration is mostly due to the loss to the chamber walls. $C_{seed}^{sus}(t)$ was also calculated based on the number concentration of the suspended particles by multiplying the average

mass in an individual bare ammonium sulfate particle (purple). C_{OA}^{sus} was the difference between the total aerosol mass with $C_{seed}^{sus}(t)$. The density of ammonium sulfate (1.77g cm^{-3}) and the SOA (1.3 g cm^{-3}) were applied during the calculation.

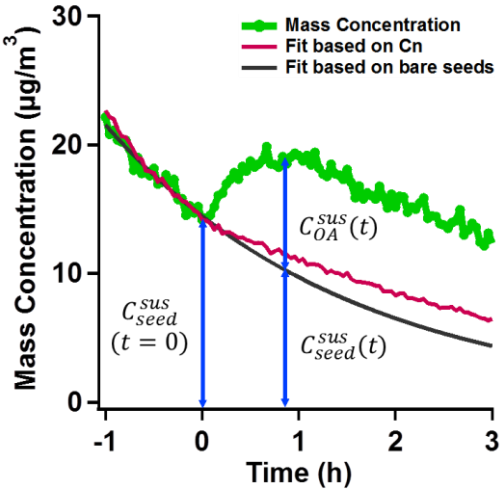

Figure 2.8 The particle wall loss correction of the formed SOA based on bare ammonium sulfate seeds and the number concentration of the suspended particles. The mass concentrations of suspended particles were only calculated with unit density.

As shown in figure 2.9, HR-AMS measured the concentration of organics (green), sulfate (red) and ammonium (Orange). Before the SOA production at 0h, the data showed there were only ammonium sulfate and almost no organics. When the reaction started, SOA condensed on the particles and the organic signal rose. Subsequently we observed a steady increase of organic mass. At 1h, particle wall loss caused the organic concentration to decrease matching the observation from the SMPS. We also observed that both the signal of sulfates and ammonium increased in the first 20mins. This may be due to the increase of the collection efficiency of particles as the organics coated on the seed. The other possible reason is that the size increase of the particles may increase the transmission efficiency in the lens system of AMS. We calculated the SOA concentration

(blue) following equation 2.3. Here, the ratio of C_{OA}^{sus} to C_{seed}^{sus} is equal to the ratio of the organic to seeds (ammonium and sulfate) concentration in suspended particles. C_{seed}^{sus} $(t = 0)$ was obtained from the SMPS measurement at time 0h.

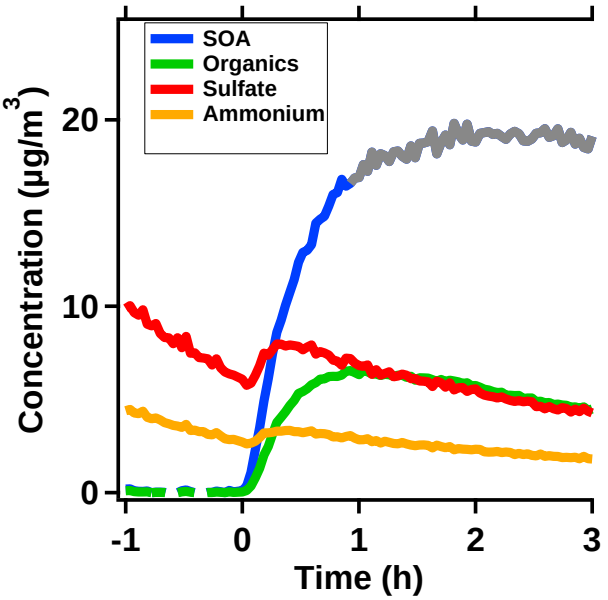

Figure 2.9 Organic, sulfate and ammonium concentration of particles measured from HR-AMS during the SOA formation experiment from PD. SOA concentration was calculated after particle wall loss correction.

2.3.4 SOA mass yield of pinanediol

Combining the SOA concentration with the reacted PD which was measured by the PTR-MS before, we calculated the SOA mass yield following equation 1. The results are plotted in figure 2.10. The initial PD concentraion is 5ppbv (37.5µg m^{-3}). The green curve shows the production of SOA vs the amount of PD reacted. SOA increased slowly at the beginning because condensible vapors needed to reach saturation before it could condense on the seed particles. At this period, most species in the SOA are ELVOCs. Further condensation of SVOC vapors to the particles drove increasing SOA yields followed. The SOA mass yield (blue) increased steadily. This can be explained by

partitioning theory. When SOA was very low, the SVOC partitioning coefficient was small. Only a few portion of the SVOCs partitioned into the particles. The SOA mass yields were low at this time. As the SOA mass increased, higher C_{OA} drove higher partitioning; more compounds partitioned into the aerosol phase and the SOA mass yields increased. The change is more obvious when plotting the SOA mass yields over the SOA concentration in figure 2.11.

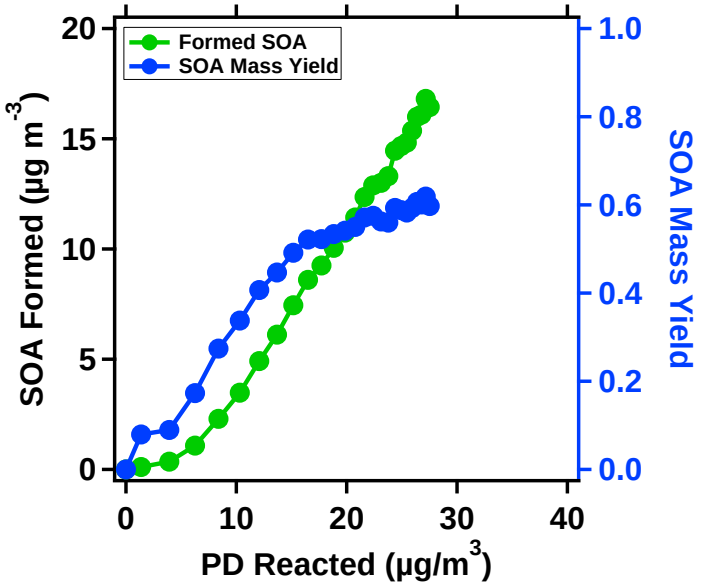

Figure 2.10 SOA mass yield from PD with HONO as OH radicals source. The intitial concentration of PD is 37.5µg m^{-3} (5ppbv).

Figure 2.11 sumarizes the SOA mass yield from several experiments with different initial concentrations, 1,2,4,5,6 and 12 ppbv under similar experimental conditions. SOA yields for all 6 experiments lie on one curve. Higher intitial PD concentraion resulted in more SOA in the high SOA mass region of the yield curve. The observed SOA yields from PD ranged from 0.1 to 1 with the different SOA loadings. The value is much higher than a-pinene. When SOA loading is 20 µg m^{-3}, the SOA mass yields from a-pinene are around

0.1-0.2. The SOA mass yield observed from PD in this study was around 0.7, roughly 5 times larger. One reason is that PD has two extra OH groups, much less volatile and more oxidized than a-pinene. This made the oxidition products from PD less volatile and more oxidized than those products from a-pinene, which easily condensed on the particles. This is confirmed by the elemental analysis from HRAMS in the next section. Our data are consistant with ~10% of the SOA with low volatility that could dirve new particle formation (Schobesberger et al., 2013;Riccobono et al., 2014).

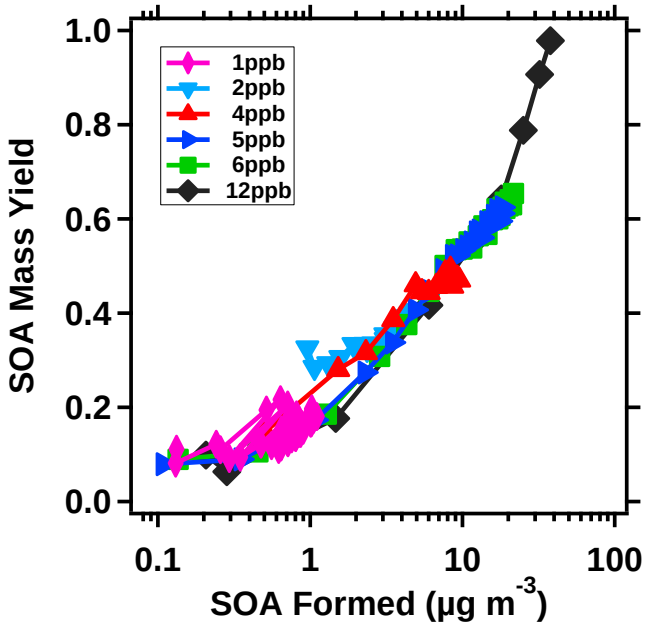

Figure 2.11 SOA mass yields from PD over the SOA production with serveral initial concentration, 1,2,4,5,6 and 12 ppbv.

2.3.5 Elemental analysis from HR-AMS.

HR-AMS measurement allowed us to use the ion fragment composition and concentrations to estimate the oxidation state of the SOA formed. Figure 2.12 shows the change of f44 and f43, the ratio of fragment org44 (CO_2^+) and org43 (mostly $C_2H_3O^+$) to

the total organic aerosols, respectively. Both f44 and f43 had relatively high values at the beginning and then decreased during the first 10 mins. After that, f43 remained almost constant, while f44 increased slowly. As discussed above, there was only a small amount of SOA formed at the beginning. At that time, only the compounds with very low volatility (ELVOCs) could condense on the particles. These ELVOCs were highly oxidized and may have more than 1 carbonyl acid group, which contributed to the CO_2^+ (*m/z*=44) fragment concentration. This is why we observed very high f44 initially. Those products could also generate $C_2H_3O^+$ fragment which dominated *m/z*=43 during this period. The slow increase of f44 after the first 10 minutes may be due to the further oxidation of the oxidized products in the gas phase, produced following the fragmentation pathway.

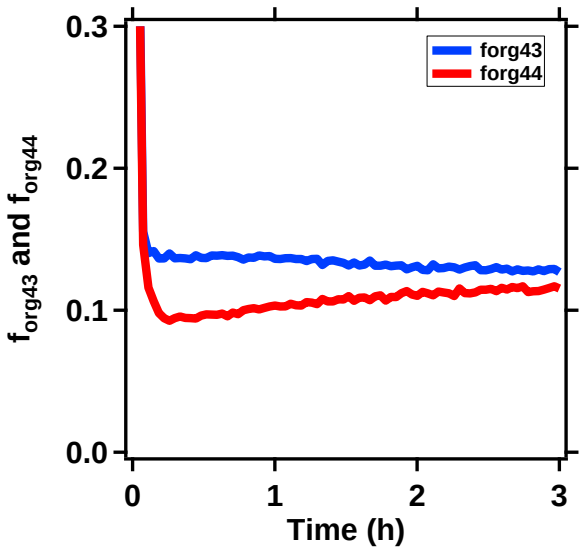

Figure 2.12. The change of f44 and f43 of SOA formed from PD oxidation.

The elemental composition, the ratio of oxygen to carbon (O:C) and hydrogen to carbon (H:C) gave the direct information about the change of hydrogen and oxygen atoms in the product molecules during the oxidation. In figure 2.13, O:C (red) deceased and H:C

(blue) increased at the beginning. The overall carbon oxidation states (OSc = 2 O:C - H:C, black) shows a steady decrease. The reason is same as the change of f44. ELVOCs contributed to most of the formed SOA mass during this period. They have more oxygen, less hydrogen. So the average OSc was high. After that, the ratio of O:C kept increasing during the reaction, while the ratio of H:C was decreasing. This may be also due to the further oxidation of the oxidized products in the gas phase.

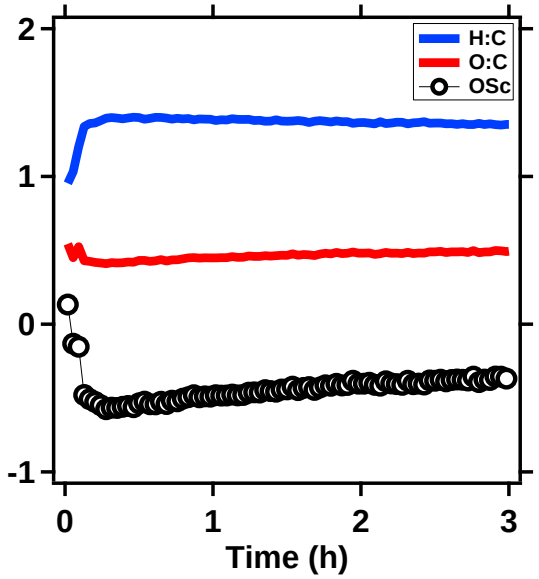

Figure 2.13 The elemental ratio, H:C and O:C, and the average carbon oxidation state, OSc of SOA formed from PD oxidation.

Figure 2.14 summarizes the observed OSc of the SOA from PD with initial concentration at 4, 5, 6 and 12 ppb in the right panel. It clearly shows OSc decreased when SOA mass increased. The increase of OSc at the end may be due to the further oxidation of the products. We also observed that SOA with smaller PD initial concentration showed higher OSc at the same SOA concentration. When PD concentration was low, the

oxidation products may have more chances to react with HO radicals and become more oxidized than the products with higher PD concentration.

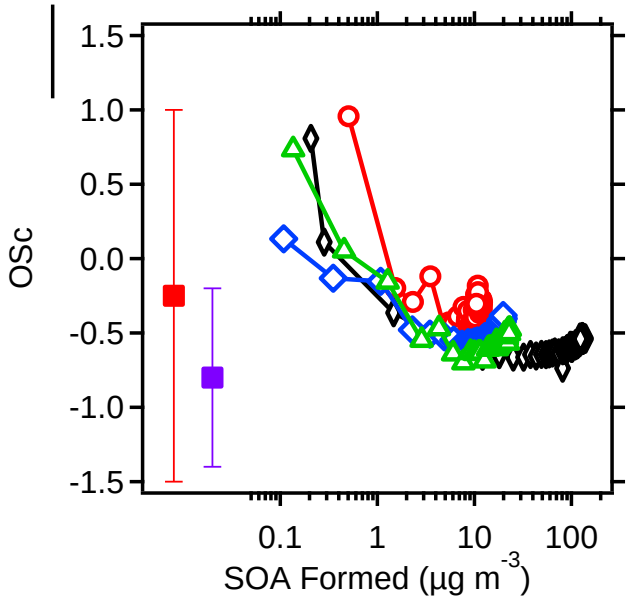

Figure 2.14 OSc of the SOA from PD with initial concentration at 4,5,6 and 12 ppb on the right panel. The left panel shows the OSc of the oxidation products of PD in the clusters observed in CLOUD, which contained 1 (red) and 4 (blue) C_{10} organics.

The OSc in this study matches the results from CLOUD (the left panel). In CLOUD, the observed oxidized organics in the clusters showed molecular composition $C_{10}H_xO_y$, where x = 12, 14, 16 and y = 2–12 (Schobesberger et al., 2013). They observed 4 progressive bands, which contains 1-4 C_{10} organics, respectively. The average carbon oxidation states of all the organics in the first band (one C_{10} organic, red) and fourth bond (four C_{10} organic, blue) are reproduced in the left panel. The OSc in the first band showed the high value, and then started to decrease and reached near to a constant, around -0.8, after the fourth band. The decrease of OSc with increasing clusters size is consistent with

what we observed in this study. The OSc of the SOA from PD in this study was around -0.7, which matched the results from CLOUD.

2.3.5 Represent oxidation products from PD in the two-dimensional volatility basis set.

Following the procedures in the literature (Presto and Donahue, 2006;Donahue et al., 2011a), the distribution of volatility and oxidation state were calculated and plotted in the two-dimensional volatility-oxidation space in figure 2.15. Organics are classified as ELVOCs, LVOCs, SVOCs or intermediate volatility organic compounds (IVOCs). PD is shown with a yellow dot. The blue contour shows the oxidation products from the PD. The major oxidized products move to top left, which show lower volatility and higher OSc. This is mostly due to the addition of oxygen atom into the products. However, the products locating on the right side of PD shows higher OSc, also higher volatility. They may be generated by two possible reaction pathways. One is the fragmentation, which breaks the carbon backbone and produce smaller molecules with higher volatility than the reactants. Another pathway may be converting alcohol group to carbonyl group (ketone or aldehyde) which makes the products less polar and higher volatile. For example, OPC, the possible oxidation product from PD may follow this pathway and show higher volatility than PD. The products near to the top left corner may contribute to the nucleation observed in CLOUD. Their saturation concentrations are lower than 0.1 $\mu g\ m^{-3}$; The OSc of these products are from 0 to 1. They represent around 10% of total SOA mass.

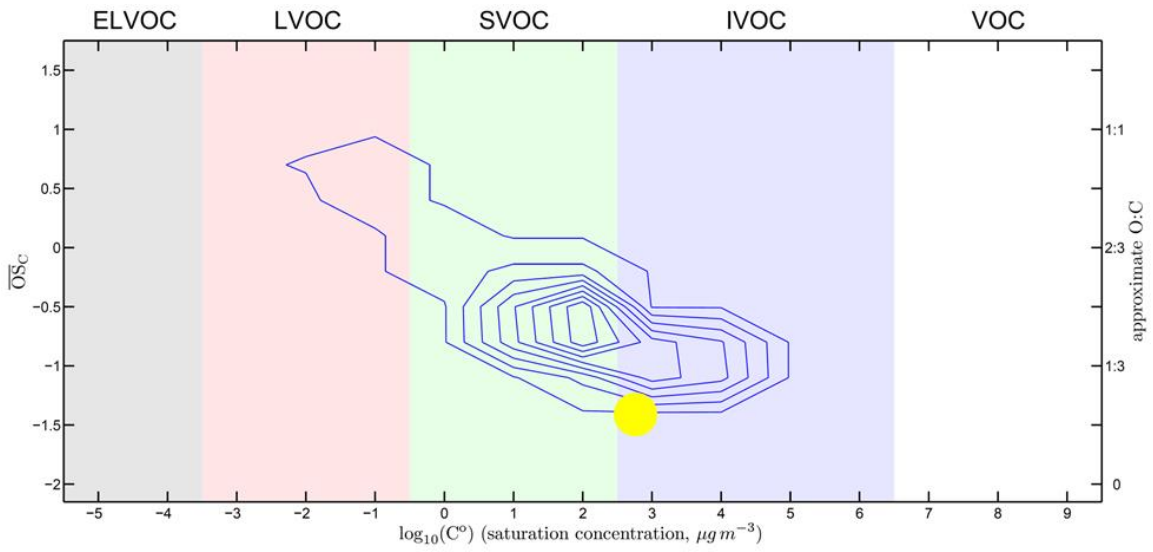

Figure 2.15 Representation of the oxidation products from PD in the 2D volatility basis set. PD is shown with a yellow dot. Blue contours show the oxidation products from PD in this study.

2.4 Conclusions

Our studies show that it is very important to correct the vapor loss of SVOCs when studying their SOA formation. In the case of PD, the SOA mass yields would be 7 times lower without the correction for PD wall loss. We observed very slow and negligible release of PD from the chamber walls under the experimental conditions in this study. The significant release of PD was observed when heating up the chamber from 13 ^{o}C to 44 ^{o}C. There was 3 times increase in PD concentraion. The distribution of oxidation products in the 2D volatility basis set shows that around 10% of oxidation products of PD may contribute to the nucleation, which is consistant to what observe in CLOUD. The OSc of the SOA from PD is around -0.7, matching the results from CLOUD.

2.5 References

Donahue, N. M., Epstein, S. A., Pandis, S. N., and Robinson, A. L.: A two-dimensional volatility basis set: 1. organic-aerosol mixing thermodynamics, Atmos. Chem. Phys., 11, 3303-3318, 2011a.

Donahue, N. M., Trump, E. R., Pierce, J. R., and Riipinen, I.: Theoretical constraints on pure vapor-pressure driven condensation of organics to ultrafine particles, Geophys Res Lett, 38, L16801, 2011b.

Donahue, N. M., Henry, K. M., Mentel, T. F., Kiendler-Scharr, A., Spindler, C., Bohn, B., Brauers, T., Dorn, H. P., Fuchs, H., Tillmann, R., Wahner, A., Saathoff, H., Naumann, K.-H., Möhler, O., Leisner, T., Müller, L., Reinnig, M.-C., Hoffmann, T., Salo, K., Hallquist, M., Frosch, M., Bilde, M., Tritscher, T., Barmet, P., Praplan, A. P., DeCarlo, P. F., Dommen, J., Prévôt, A. S. H., and Baltensperger, U.: Aging of biogenic secondary organic aerosol via gas-phase OH radical reactions, PNAS, 109, 13503-13508, 2012.

Ehn, M., Thornton, J. A., Kleist, E., Sipila, M., Junninen, H., Pullinen, I., Springer, M., Rubach, F., Tillmann, R., Lee, B., Lopez-Hilfiker, F., Andres, S., Acir, I.-H., Rissanen, M., Jokinen, T., Schobesberger, S., Kangasluoma, J., Kontkanen, J., Nieminen, T., Kurten, T., Nielsen, L. B., Jorgensen, S., Kjaergaard, H. G., Canagaratna, M., Maso, M. D., Berndt, T., Petaja, T., Wahner, A., Kerminen, V.-M., Kulmala, M., Worsnop, D. R., Wildt, J., and Mentel, T. F.: A large source of low-volatility secondary organic aerosol, Nature, 506, 476-479, 2014.

Henry, K. M., and Donahue, N. M.: Photochemical aging of α-pinene secondary organic aerosol: Effects of OH radical sources and photolysis, The Journal of Physical Chemistry A, 2012.

Hildebrandt, L., Donahue, N. M., and Pandis, S. N.: High formation of secondary organic aerosol from the photo-oxidation of toluene, Atmos. Chem. Phys., 9, 2973-2986, 2009.

Kanakidou, M., Seinfeld, J. H., Pandis, S. N., Barnes, I., Dentener, F. J., Facchini, M. C., Dingenen, R. V., Ervens, B., Nenes, A., Nielsen, C. J., Swietlicki, E., Putaud, J. P., Balkanski, Y., Fuzzi, S., Horth, J., Moortgat, G. K., Winterhalter, R., Myhre, C. E. L., Tsigaridis, K., Vignati, E., Stephanou, E. G., and Wilson, J.: Organic aerosol and global climate modelling: a review, Atmos. Chem. Phys., 5, 1053-1123, 2005.

Kirkby, J., Curtius, J., Almeida, J., Dunne, E., Duplissy, J., Ehrhart, S., Franchin, A., Gagne, S., Ickes, L., Kurten, A., Kupc, A., Metzger, A., Riccobono, F., Rondo, L., Schobesberger, S., Tsagkogeorgas, G., Wimmer, D., Amorim, A., Bianchi, F., Breitenlechner, M., David, A., Dommen, J., Downard, A., Ehn, M., Flagan, R. C., Haider, S., Hansel, A., Hauser, D., Jud, W., Junninen, H., Kreissl, F., Kvashin, A., Laaksonen, A., Lehtipalo, K., Lima, J., Lovejoy, E. R., Makhmutov, V., Mathot, S., Mikkila, J., Minginette, P., Mogo, S., Nieminen, T., Onnela, A., Pereira, P., Petaja, T., Schnitzhofer, R., Seinfeld, J. H., Sipila, M., Stozhkov, Y., Stratmann, F., Tome, A., Vanhanen, J., Viisanen, Y., Vrtala, A., Wagner, P. E., Walther, H., Weingartner, E., Wex, H., Winkler, P. M., Carslaw, K. S., Worsnop, D. R., Baltensperger, U., and Kulmala, M.: Role of sulphuric acid, ammonia and galactic cosmic rays in atmospheric aerosol nucleation, Nature, 476, 429-433, 2011.

Matsunaga, A., and Ziemann, P. J.: Gas-Wall Partitioning of Organic Compounds in a Teflon Film Chamber and Potential Effects on Reaction Product and Aerosol Yield Measurements, Aerosol Science and Technology, 44, 881-892, 2010.

Nakao, S., Tang, P., Tang, X., Clark, C. H., Qi, L., Seo, E., Asa-Awuku, A., and Cocker Iii, D.: Density and elemental ratios of secondary organic aerosol: Application of a density prediction method, Atmospheric Environment, 68, 273-277, 2013.

Pope, C. A., Ezzati, M., and Dockery, D. W.: Fine-Particulate Air Pollution and Life Expectancy in the United States, New England Journal of Medicine, 360, 376-386, 2009.

Presto, A. A., and Donahue, N. M.: Investigation of α-Pinene + Ozone Secondary Organic Aerosol Formation at Low Total Aerosol Mass, Environmental Science & Technology, 40, 3536-3543, 2006.

Riccobono, F., Schobesberger, S., Scott, C. E., Dommen, J., Ortega, I. K., Rondo, L., Almeida, J., Amorim, A., Bianchi, F., Breitenlechner, M., David, A., Downard, A., Dunne, E. M., Duplissy, J., Ehrhart, S., Flagan, R. C., Franchin, A., Hansel, A., Junninen, H., Kajos, M., Keskinen, H., Kupc, A., Kürten, A., Kvashin, A. N., Laaksonen, A., Lehtipalo, K., Makhmutov, V., Mathot, S., Nieminen, T., Onnela, A., Petäjä, T., Praplan, A. P., Santos, F. D., Schallhart, S., Seinfeld, J. H., Sipilä, M., Spracklen, D. V., Stozhkov, Y., Stratmann, F., Tomé, A., Tsagkogeorgas, G., Vaattovaara, P., Viisanen, Y., Vrtala, A., Wagner, P. E., Weingartner, E., Wex, H., Wimmer, D., Carslaw, K. S., Curtius, J., Donahue, N. M., Kirkby, J., Kulmala, M., Worsnop, D. R., and Baltensperger, U.: Oxidation Products of Biogenic Emissions Contribute to Nucleation of Atmospheric Particles, Science, 344, 717-721, 2014.

Schobesberger, S., Junninen, H., Bianchi, F., Lönn, G., Ehn, M., Lehtipalo, K., Dommen, J., Ehrhart, S., Ortega, I. K., Franchin, A., Nieminen, T., Riccobono, F., Hutterli, M., Duplissy, J., Almeida, J., Amorim, A., Breitenlechner, M., Downard, A. J., Dunne, E. M., Flagan, R. C., Kajos, M., Keskinen, H., Kirkby, J., Kupc, A., Kürten, A., Kurtén, T., Laaksonen, A., Mathot, S., Onnela, A., Praplan, A. P., Rondo, L., Santos, F. D., Schallhart, S., Schnitzhofer, R., Sipilä, M., Tomé, A., Tsagkogeorgas, G., Vehkamäki, H., Wimmer, D., Baltensperger, U., Carslaw, K. S., Curtius, J., Hansel, A., Petäjä, T., Kulmala, M., Donahue, N. M., and Worsnop, D. R.: Molecular understanding of atmospheric particle formation from sulfuric acid and large oxidized organic molecules, Proceedings of the National Academy of Sciences, 110, 17223-17228, 2013.

Seinfeld, J. H., and Pankow, J. F.: ORGANIC ATMOSPHERIC PARTICULATE MATERIAL, Annual Review of Physical Chemistry, 54, 121-140, 2003.

Seinfeld, J. H., and Pandis, S. N.: Atmospheric chemistryand physics — from air pollution to climate change, 2nd ed., John Wiley & Sons, New York, 2006.

Solomon, S. Q., D.; Manning, M.; Alley, R. B.; Berntsen, T.; Bindoff, N. L.; Chen, Z.; Chidthaisong, A.; Gregory, J. M.; Hegerl, G. C.: Climate change 2007: The physical science basis, contribution of working group 1 to the fourth assessment report of the Intergovernmental Panel on Climate Change, 2007.

Trump, E. R., Riipinen, I., and Donahue, N. M.: Interactions between atmospheric ultrafine particles and secondary organic aerosol mass: a model study, Boreal Environ. Res., 19, 00-00, 2014.

Zhang, Q., Jimenez, J. L., Canagaratna, M. R., Allan, J. D., Coe, H., Ulbrich, I., Alfarra, M. R., Takami, A., Middlebrook, A. M., Sun, Y. L., Dzepina, K., Dunlea, E., Docherty, K., DeCarlo, P. F., Salcedo, D., Onasch, T., Jayne, J. T., Miyoshi, T., Shimono, A., Hatakeyama, S., Takegawa, N., Kondo, Y., Schneider, J., Drewnick, F., Borrmann, S., Weimer, S., Demerjian, K., Williams, P., Bower, K., Bahreini, R., Cottrell, L., Griffin, R. J., Rautiainen, J., Sun, J. Y., Zhang, Y. M., and Worsnop, D. R.: Ubiquity and dominance of oxygenated species in organic aerosols in anthropogenically-influenced Northern Hemisphere midlatitudes, Geophys Res Lett, 34, L13801, 2007.

Zhao, Y., Hennigan, C. J., May, A. A., Tkacik, D. S., de Gouw, J. A., Gilman, J. B., Kuster, W. C., Borbon, A., and Robinson, A. L.: Intermediate-Volatility Organic Compounds: A Large Source of Secondary Organic Aerosol, Environmental Science & Technology, 48, 13743-13750, 2014.

Chapter 3

Vapor wall loss of semi-volatile organic compounds in Teflon chamber

Abstract

We have investigated the vapor wall loss of semi-volatile organic compounds (SVOCs) in the CMU smog chamber. Wall loss is a key factor influencing organic aerosols behavior in chamber experiments. Direct treatment of particle wall loss is straightforward. However, little knowledge is available about vapor wall loss, deposition of organic vapors on or into Teflon chamber walls. Matzunaga and Ziemann showed that volatile organic vapors could sorb reversibly into Teflon chamber walls, but direct observations of SVOC vapor wall loss are lacking. We studied the passive decays of seven SVOCs with known saturation concentration, including alkanes (hexacosane, pentacosane, docosane, eicosane, d_{62}-squalane), an organic acid (oleic acid), and a polyol (levoglucosan) in single-component and binary-component (organic) systems, using ammonium sulfate (AS) seeds to constrain the particle wall loss. SVOCs coating AS seeds sustain SVOC vapors at or near their saturation concentration, so the mass loss of organics from the suspended particles reflects vapor wall loss. For all organics studied here, the ratio of organics to sulfate in the suspended particles (org:sulf) decreased steadily, clearly indicating significant vapor wall loss. Our results showed that the wall loss rates of SVOCs vapor were significant and consistently proportional to vapor concentrations in the gas phase. The vapor loss of the alkanes increased with decreasing carbon number. Eicosane had the highest loss rate while

hexacosane showed a quite small loss rate. Pure oleic acid showed a larger loss rate than in the mixture with d_{62}-squalane, and the loss rate of oleic acid in the mixture was positively correlated with the fraction of oleic acid in the mixture.

3.1 Introduction

Particulate matter (PM) in the atmosphere has important impacts on human health and life expectancy (Pope et al., 2009) and also influences on Earth's climate by absorbing and scattering radiation (Solomon, 2007). Secondary organic aerosol (SOA) represents a significant fraction of the organic mass in PM.(Zhang et al., 2007) Semi-volatile organic compounds (SVOCs), which exist in significant fractions in both condensed and vapor phases, is a very important category of compounds associated with organic aerosols. More than two decades of research supports an understanding that SOA consists largely of SVOCs (Pankow, 1994;Odum et al., 1996;Kamens et al., 1999;Donahue et al., 2006). Though discovery of oligomers in SOA (Kalberer et al., 2004) and more recently extremely low volatility organics (ELVOC) formed in the gas phase (Ehn et al., 2014;Kokkola et al., 2014) has called into question what fraction of SOA formation proceeds via SVOCs. Conversely, POA was long treated as being non-volatile, but extensive evidence has shown that the majority of POA consists of SVOCs (Robinson et al., 2007;Grieshop et al., 2009).

Smog chambers have been extensively used to study SOA formation, chemical reaction and physical properties.(Stern et al., 1987;Pandis et al., 1991;Zhang et al., 1992;Odum et al., 1997;Hoffmann et al., 1997;Presto et al., 2005b;Presto et al., 2005a) The interaction between SVOC vapor with Teflon chamber wall and suspended particles is a key factor influencing organic aerosol formations and behaviors in chamber experiments. The loss of organic vapors to the Teflon chamber wall reduces the condensation of vapors to suspended particles and thus the

apparent SOA mass yield. Furthermore, if vapor wall losses are selective, this can bias the chemical composition and properties of formed SOA. Direct treatment of particle wall loss is straightforward (Stanier et al., 2008). Recently more attention has been given to the vapor wall loss due to the condensation of organic vapors on or into Teflon chamber walls (McMurry and Grosjean, 1985;Matsunaga and Ziemann, 2010;Loza et al., 2010;McVay et al., 2014;Zhang et al., 2014a;Zhang et al., 2014b;Yeh and Ziemann, 2014). Apparent SOA yields can be biased low by a factor of four due to vapor wall loss (Zhang et al., 2014a). VOC vapors, including n-alkanes, 1-alkenes, 2-alcohols, and 2-ketones, could be sorbed reversibly into Teflon chamber walls (Matsunaga and Ziemann, 2010). 2,3-epoxy-1,4-butanediol, and glyoxal showed the similar wall loss behaviors (Loza et al., 2010). Organonitates also showed significant vapor wall loss (Yeh and Ziemann, 2014).

Our goal is to directly quantify the loss of SVOCs vapor to the Teflon chamber walls. Matzunaga and Ziemann measured the fractions of the VOCs present in the gas phase at equilibrium (Matsunaga and Ziemann, 2010). By design, they studied losses for relatively volatile compounds well below saturation. This was to avoid particle formation and condensation to the walls driven solely by nucleation of a condensed phase on the walls. Broadly, the compounds they studied can be classified as Intermediate Volatility Organic Compounds (IVOCs). They injected a carefully quantified aliquot of various IVOCs into an otherwise empty chamber, waited for the chamber to become well mixed, and then measured the gas-phase concentration. They observed a deficit in the gas phase inversely correlated with vapor pressure but also related to the IVOC molecular structure. Furthermore, they were able to recover a fraction of any missing material by flushing the chamber and re-filling it with clean air. They concluded that the results were consistent with organic vapors reaching an absorptive equilibrium within a thin

layer of disordered polymer at the Teflon surface. Though the organics presumably have a very high activity coefficient for sorption within the Teflon matrix, the extremely large overall mass of this layer (compared with 10-100 μg m^{-3} levels of organics in SOA conditions) resulted in significant mass uptake for the IVOCs, consistent with a sorptive equilibrium given by

$$F_{wall} = 1/(1 + C_{wall} / C^{o})$$

where C^{o} is the saturation concentration of the IVOC and C_{wall} is an effective wall concentration for partitioning. Broadly, they found 2 mg m^{-3} < C_{wall} < 25 mg m^{-3} depending on structure.

The Matsunaga and Ziemann findings can be extrapolated to SVOCs. The implication is that the large majority of SVOCs will reside in the wall at equilibrium. For example an SVOC with C* ~ 10 μg m^{-3} would have F_{wall} = 0.999, more than 99% of SVOCs vapor may be lost to the Teflon wall when reaching equilibrium. The vapor loss of SVOCs to the chamber walls may be considered as quasi-irreversible. Therefore, it is challenging to measure SVOC vapor concentrations, especially as the wall equilibration is thought to occur quickly. Zhang et al. used chemical ionization mass spectrometry (CIMS) to track the concentration of 25 oxidized organic compounds generated from the photooxidation of SOA precursors (Zhang et al., 2014b), but reported data after an hour or so of SOA formation. Yeh and Ziemann monitored the vapor loss of a suite of synthesized alkyl nitrates to constrain the loss of alkyl nitrates from C_8−C_{14} n-alkanes reacted with OH radicals in the presence of NO_x (Yeh and Ziemann, 2014), finding that the inferred wall loss of semi-volatile nitrates was consistent with expectations. In our study, we probed SVOC vapor wall loss through the measurement of suspended particles coated with SVOCs. Our objective was to establish a gas-particle equilibrium at saturation and then to follow mass loss from particles. The well-established measurement methods for particles allowed us to

measure the loss of SVOC vapors for a range of molecules. We studied seven SVOCs with known saturation concentration, including alkanes (hexacosane, pentacosane, docosane, eicosane, d_{62}-squalane), a carboxylic acid (oleic acid), and a polyalcohol (levoglucosan) in single-component and binary-component (organic) systems. The objective of this study is to map the vapor wall loss behaviors of SVOCs with well-known model compounds.

3.2 Methods and Materials

The experimental design is conceptually straightforward as shown in scheme 3.1. We coated ammonium sulfate (AS) seeds with a SVOC in a Teflon chamber. After SVOCs were introduced into the chamber, they either existed in the gas phase, condensed on the ammonium sulfate particles, or were lost to the Teflon chamber wall. We used enough seeds for SVOC vapors to reach the equilibrium with the particles quickly compared to the wall loss timescale. SVOC vapors were continuously lost to the Teflon chamber walls, but the organic coated particles sustained the SVOCs in the gas phase at or near their saturation concentration. The mass loss of organics from the suspended particles, which is the difference between the evaporation and condensation, thus reflects SVOCs vapor wall loss. The loss of SVOCs from the particles decreased the organic fraction in the particles and caused particle shrinking. This allowed us to calculate the SVOC vapor wall loss by tracing the organic mass change of particles, by measuring the organic to sulfate ratio (org:sulf) with an aerosol mass spectrometry.

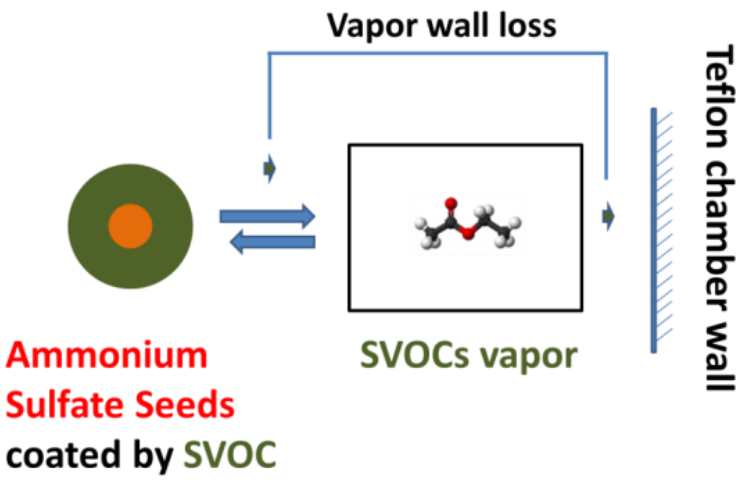

Scheme 3.1 The partitioning of SVOCs between the gas phase, particle phase and Teflon chamber wall.

We measured mass concentrations on the particles with a high resolution time-of-flight aerosol mass spectrometer (HR-ToF-AMS). We used org:sulf because it is conserved during particle wall loss and precisely measured even when the particle collection efficiency is less than 1 and not constant. Through model simulations of gas-particle-wall partitioning of SVOCs, we calculated the vapor wall loss rate.

Experiments were performed at the Carnegie Mellon University (CMU) Smog Chamber, a 10 m^3 Teflon bag suspended in a temperature controlled room. Many details of the experimental procedures were described in a previous paper (Hildebrandt et al., 2009). Only a brief description is provided here. Prior to experiments the bag was cleaned by flushing with clean, dry air and exposed to high temperatures (~35 °C) and UV irradiation. After cleaning, the chamber was maintained at a constant temperature.

All experiments were performed with ammonium sulfate ($(NH_4)_2SO_4$, Sigma Aldrich, 99.99%) seed particles. The seeds were formed by atomizing a 1 g/L $(NH_4)_2SO_4$ in a water solution to form droplets that passed through a diffusion dryer and a neutralizer before they entered the

chamber. Glucose was mixed in solution with AS and added into chamber with the same procedure as AS. SVOCs were injected into the chamber by gentile vaporization and then condensed on the AS seeds with minimal nucleation. A small, resistive metal heater enclosed in a stainless steel sheath was used to evaporate the organic material inside the chamber. The organic material was placed on the stainless steel surface before the heater was inserted into the chamber on the end of a long tube. With a flow of clean, dry dispersion air used to mix the chamber, the heater was power-cycled until the organic material completely evaporated.

Particle number and volume inside the chamber were measured using a scanning mobility particle sizer (SMPS, TSI classifier model 3080, CPC model 3772 or 3010). Particle mass was measured by a high resolution time-of-flight aerosol mass spectrometer (HR-ToF-AMS, Aerodyne Research, Inc.). Single-particle mass spectra for particles with Dva $\geq$180 nm were taken with an HR-ToF-AMS operated in light scattering single particle (LSSP) mode, which has been described in detail before (Robinson et al., 2013). We operated the HR-ToF-AMS according to the common protocol with the vaporizer temperature at 600 ^{o}C. We collected mass spectra and particle time-of-flight (pToF) measurements in V-mode. For all experiments, the HR-ToF-AMS alternated between V-mode and LSSP mode for 60s each.

3.3 Results and discussion

3.3.1 Observation of vapor wall loss of oleic acid and glucose.

First we shall consider one non-volatile and one semi-volatile organic in detail: oleic acid and glucose. Oleic acid is one example of SVOCs. Glucose is considered a non-volatile or extremely low volatility organic compound (ELVOC) that barely exists in gas phase. So the vapor wall loss of glucose should be negligible. Figure 3.1 shows the results of experiments with glucose (a) and

oleic acid (b). AS particles coated by glucose were prepared by nebulizing an aqueous solution of glucose and AS. The passive decay began at 0h, 5mins (the mixing time of our chamber) after the seeding step was completed. We tracked the change of particles with the SMPS and AMS. We did not observe any significant change of mean particle volume (black), which was calculated from the SMPS measurement, or org:sulf (green), which was calculated from the AMS measurement. This is consistent with the fact that glucose has no or very little vapor wall loss. In contrast to glucose, oleic acid showed a clear decrease in both org:sulf and average particle volume over time. In Figure 3.1b, oleic acid was injected into the chamber with the vaporizer between -0.3 and 0h, in presence of AS seeds. The passive decay started at 0h. Both mean particle volume (black) and org:sulf (green) decreased steadily afterwards. The results clearly indicated that oleic acid evaporated continuously from the particles. The particles lost half oleic acid in around one hour. Considering that oleic acid vapors already reached the saturation concentration, 4.0 $\mu g \cdot m^{-3}$, when it started to condense on the AS seeds, the most probable, and perhaps only, destination of the lost oleic acid was the Teflon chamber wall; The oleic acid vapors were adsorbed and/or absorbed by the wall. The loss of oleic acid vapor reduced the chemical potentials of oleic acid in gas phase, and then caused the evaporation of oleic acid from particles and thus the mass loss of oleic acid on particles. The results clearly confirm that the vapor loss of SVOCs are significant and can be observed. Org:sulf of the suspended particles is a very robust parameter to track the wall loss of SVOC vapors in the chamber.

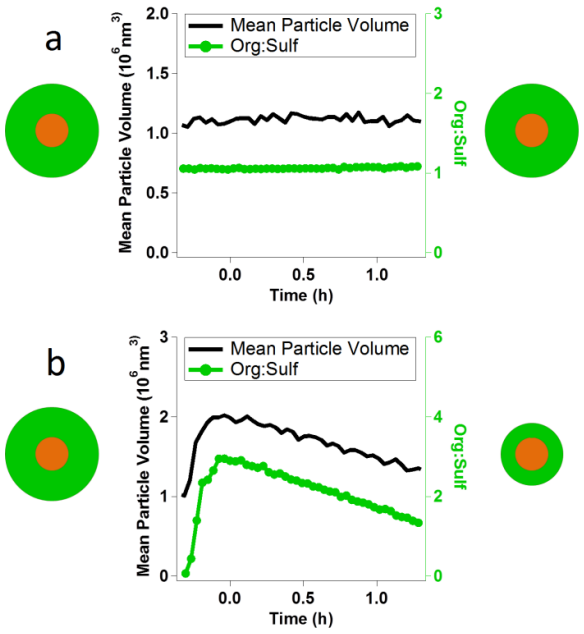

Figure 3.1 Mean particle volume (black) and org:sulf (green) of glucose (a) and oleic acid (b) coated ammonium sulfate particles. The cartoon demonstrated the change of AS seeds (red) coated with the SVOCs (green).

3.3.2 The effect of the change of org:sulf due to size dependent particle wall loss and composition

We compared the vapor loss of a nearly no-volatile soluble organic (glucose, a) and a nearly non-volatile insoluble paraffin (solid hexacosane, b), coated AS particles. As shown in Figure 3.2a, the glucose coated AS particles show almost identical mass distribution of the organic and sulfate. While, for the hexacosane coated AS particles (3.2b), smaller particles have larger organic mass fraction. Size dependent particle wall loss may alter their overall org:sulf. However, the org:sulf of both particles did not show any significate difference. So there is no indication that size dependent particle wall loss or composition influences our results.

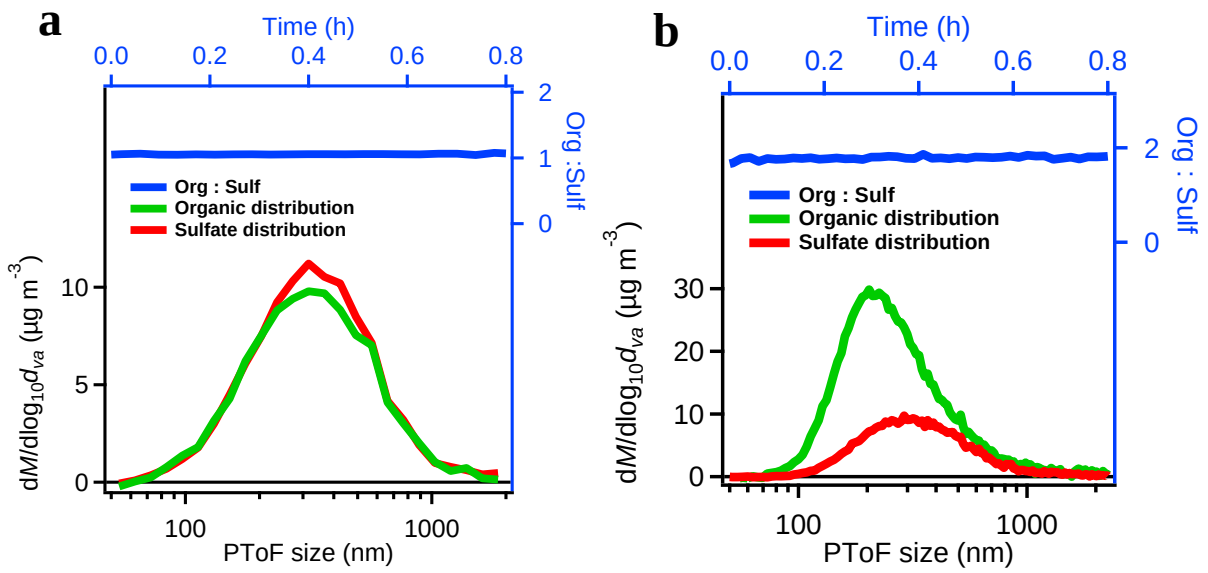

Figure 3.2 The org:sulf (blue) and the mass distribution of organic (green) and sulfate (red) of glucose (a) and hexaconsane (b) coated ammonium sulfate particles.

3.3.3 Wall loss of oleic acid vapor at the different temperature.

We also studied the vapor wall loss of oleic acid at different temperatures. The saturation concentrations of SVOCs decrease when temperature decreases. Figure 3.3 shows the change of org:sulf (green) in a chamber initially at 44 ^{o}C, but subsequently cooled to 22 ^{o}C. The org:sulf decreased much faster at 44 ^{o}C and then slowed down when the temperature was dropped to 22 ^{o}C. The different depletion rate of org:sulf clearly illustrates that the vapor wall loss rate of oleic acid is positively related to its concentration in the gas phase. Furthermore, the oscillation of org:sulf indicated that the oleic acid reached or near to the equilibrium between gas phase and particle phase. These oscillations resulted from the change of saturation concentration, which is due to the small alternated change of temperature (blue) in the chamber. When the temperature decreased, the saturation concentration of oleic acid decreased and initiated the condensation to the particles. The deposition of oleic acid increased the org:sulf. The oscillations of org:sulf for oleic acid followed every change in the temperature profiles. The peaks of the org:sulf matched

all dips in the temperature profiles. Also, we found significant organic mass increase on the particles due to oleic acid vapor condensation during the transition of the temperature from 44 ^{o}C to 22 ^{o}C. These results confirmed that the organics reached equilibrium between the gas phase and particles, and SVOCs with higher vapor concentration showed higher vapor wall loss rate.

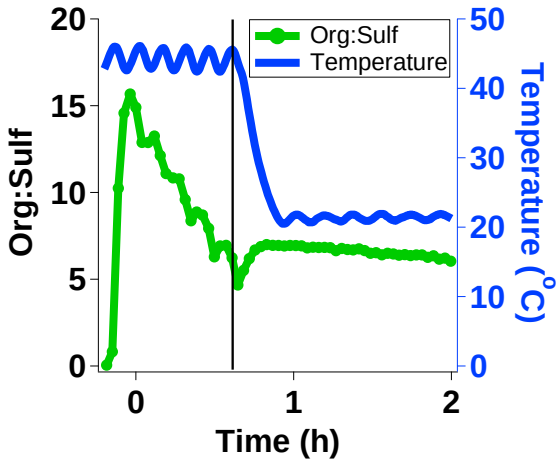

Figure 3.3 The change of org:sulf of oleic acid coated AS particles during the decrease of the temperature inside the Teflon chamber.

3.3.4 Theoretical calculation for quantification of the vapor wall loss rate.

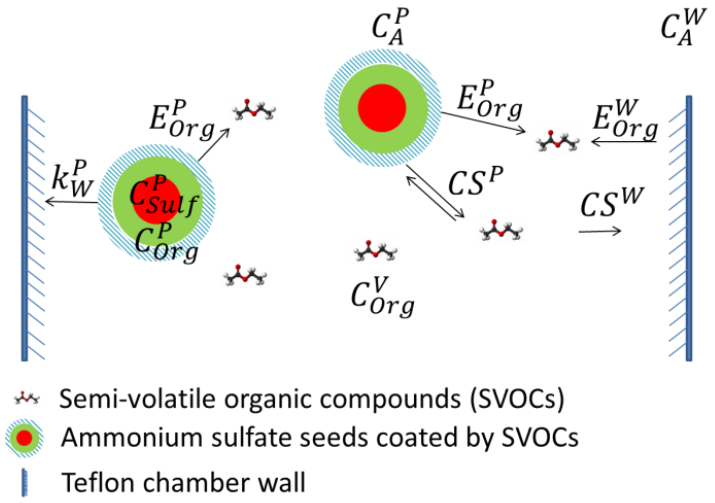

Scheme 3.2 Mass transportations of organics and sulfates among gas phase, particle phase and Teflon chamber wall.

We built a model to quantify the vapor wall loss rate. As shown in Scheme 3.2, the model considers the mass balance and kinetics of transportations of organics and sulfates (seeds) between the gas phase, particle phase and the chamber wall.

In Scheme 3.2, the net flux of organics to the gas phase from particles (E_{Org}^{P}) and from wall (E_{Org}^{W}) can be calculated with Equations 1 and 2.

$$E_{Org}^{P} = v^{*}\alpha C_{A}^{P}\left(a_{org}^{P}C_{Org}^{*} - C_{Org}^{V}\right) = CS^{P}(a_{org}^{P}C_{Org}^{*} - C_{Org}^{V}) \quad (1)$$

$$E_{Org}^{W} = v^{*}\alpha C_{A}^{W}\left(a_{org}^{W}C_{Org}^{*} - C_{Org}^{V}\right) = -CS^{W}C_{Org}^{V} \quad (2)$$

As shown, v^{*} is the mean thermal speed of the gas phase molecules. α is the accommodation coefficient. Here we considered α equal to 1 (Julin et al., 2014). C_{A}^{P} is the Fuchs surface area concentration of particles. a_{org}^{P} is the activity of the organic in the mixture on the particles. For the pure organic, a_{org}^{P} is equal to 1. C_{A}^{W} is the diffusion corrected surface area concentration (equivalent to the Fuchs corrected surface area) of the Teflon wall. a_{org}^{W} is the activity of the organic in the mixture on the wall. Considering that the vapor loss of SVOCs to the chamber walls can be considered as quasi-irreversible. So the release rate of organics from Teflon is very small. We set a_{org}^{W} equal to 0. C_{Org}^{*} is the saturation concentration of the organic in the gas phase. C_{Org}^{V} is the equilibrium concentration of the organic in the gas phase. CS^{P} and CS^{W} are the condensation sinks of the particles and the Teflon wall, respectively. We consider CS^{W} as a constant during the experiments.

We calculated the CS^{P} using equation 3 and the method in the literature (Trump et al., 2014).

$$CS^{P} = \sum_{k} N_{k}\frac{v}{4}\pi D_{P,k}\beta_{k}$$

(3)

The calculated values of CS^P during all the experiments are around 1~2 min^{-1}. CS^W was measured from the loss of sulfuric acid vapor in the Teflon chamber using a CIMS. The value was 0.108 ± 0.03 min^{-1}. For turbulent conditions the flux of vapor to the wall scales as $1/\sqrt{D}$ (McMurry and Grosjean, 1985) or $(MW)^{1/4}$, so species with MW ~ 150-300 g mol^{-1} have loss rate within 20% of each other. To simplify the calculation, here we use CS^W value from sulfuric acid directly. CS^P is 10~20 times larger than CS^W. So the evaporation of SVOCs from particles is much faster that the vapor wall loss rate. This means SVOCs evaporated from the particles are capable of covering the loss of SVOCs due to vapor wall loss, and organic coated aerosols would sustain SVOCs in the gas phase at their saturation concentration; the concentration of organics in gas phase thus remained nearly constant. So the net flux of organics to the gas phase is equal to 0. $E_{Org}^P + E_{Org}^W = 0$. After combining equation 1 and 2, we obtain:

$$C_{Org}^V = C_{Org}^* \frac{1}{1+\frac{CS^W}{CS^P}} \quad (4)$$

As shown, C_{Org}^V is positively correlated to the C_{Org}^* of the organic, and also to CS^P and CS^W. Because CS^P is 10~20 times larger than CS^W, $\frac{CS^W}{CS^P}$ is much smaller than 1, and $C_{Org}^V \approx C_{Org}^*$. Thus,

$$l_{Org}^W = -E_{Org}^W = E_{Org}^P = C_{Org}^* \frac{1}{\frac{1}{CS^P}+\frac{1}{CS^W}} \approx CS^W C_{Org}^* \quad (6)$$

For the pure compounds, the equilibrium concentration of the organic (C_{Org}^V) is approximately equal to the saturation concentration (C_{Org}^*). The loss rate of organic vapor to the wall (l_{Org}^W) is

equal to the net evaporation rate of organic from particles (E_{Org}^{P}). In addition, it has a linear relationship to vapor concentration in the gas phase (C_{Org}^{*}) and condensation sink to the chamber wall (CS^{W})

We used AS as seeds in this study to correct for the particle wall loss, but we do need to estimate the absolute flux of organics from particles to the gas phase. We based our calculation on the organic to sulfate ratio (org:sulf) measured from HR-TOF-AMS. As shown in Scheme 3.2, the decrease of sulfates was only due to the loss of particles to the Teflon wall (equation 7). The decrease of organic includes two contributions. One is due to the loss of particles, and another is the direct loss of organic vapor to the Teflon wall (equation 8).

$$\frac{dC_{Sulf}^{P}}{dt} = \ -k_{W}^{P}C_{Sulf}^{P} \quad (7)$$

$$\frac{dC_{Org}^{P}}{dt} = \ -k_{W}^{P}C_{Org}^{P} - E_{Org}^{P} \quad (8)$$

C_{Sulf}^{P} and C_{Org}^{P} are the organic and sulfate concentration in the particles, respectively. k^{P} is the particle wall loss rate. After combining equation 7 and 8, we obtain:

$$\frac{\partial(C_{Org}^{P}: C_{Sulf}^{P})}{\partial t} = \ -\frac{E_{Org}^{P}}{C_{Sulf}^{P}}$$

(9)

Because dry ammonium sulfate particles bounce on the AMS vaporizer, we must correct for particle collection efficiency (*CE* (AS) ~ 0.2). Furthermore, *CE* varies with org:sulf. Fortunately, we can measure *CE* via LSSP. Accounting for CE, we obtain:

$$l_{Org}^{W} = E_{Org}^{P} = -\frac{\partial(S_{Org}^{P}:S_{Sulf}^{P})}{\partial t}\frac{S_{Sulf}^{P}}{CE}$$

(10)

Where S_{Sulf}^{P} is the raw AMS sulfate signal. S_{Org}^{P} is the raw AMS organic signal. The loss rate of organic vapor to the wall (l_{Org}^{W}) is proportional to the change of org:sulf and the sulfate concentration during the time. We now define L_{Org}^{W} as the integrated mass loss of organic to the Teflon wall over the time t.

$$L_{Org}^{W} = -l_{Org}^{W}t = \int_{0}^{t} d\left(S_{Org}^{P}:S_{Sulf}^{P}\right)\frac{S_{Sulf}^{P}}{CE} = \sum_{i=0}^{n}\left[\Delta\left(S_{Org}^{P}:S_{Sulf}^{P}\right)\frac{S_{Sulf}^{P}}{CE}\right]_{i}$$

(11)

The total mass loss of organic, L_{Org}^{W} can be calculated by summarizing the change of org:sulf multiplied by the sulfate concentration at each very short period. After plotting the total mass loss with respect to time, we got the loss rate from the slope of the line.

3.3.5 Calculation of the vapor wall loss rate of oleic acid and levogucosan.

Figure 3.4a shows the concentrations of organic and sulfates measured with the HR-AMS. The collection efficiency was calculated based on the ratio of the number that produced a signal in the mass detector to the particles counted by the laser. In Figure 3.4b, the org:sulf, in blue in the equation, were calculated based on the concentrations of organic and sulfate. The corrected sulfate concentration, in red, was calculated by dividing the original sulfate concentration by CE determined by a linear fit to CE for t≥0h. Then We calculated the vapor loss each minute with the decrease of the org:sulf and the average of sulfate concentration, following equation 11. V

mode measurements from HR-AMS are one minute averages, so we analyzed date on 1min time basis. The total vapor loss (L_{Org}^{W}) was the sum over every minute period.

$$L_{Org}^{W} = -l_{Org}^{W} t = \sum_{i=0}^{n} [\Delta(S_{Org}^{P} : S_{Sulf}^{P}) \frac{S_{Sulf}^{P}}{CE}]_{i}$$

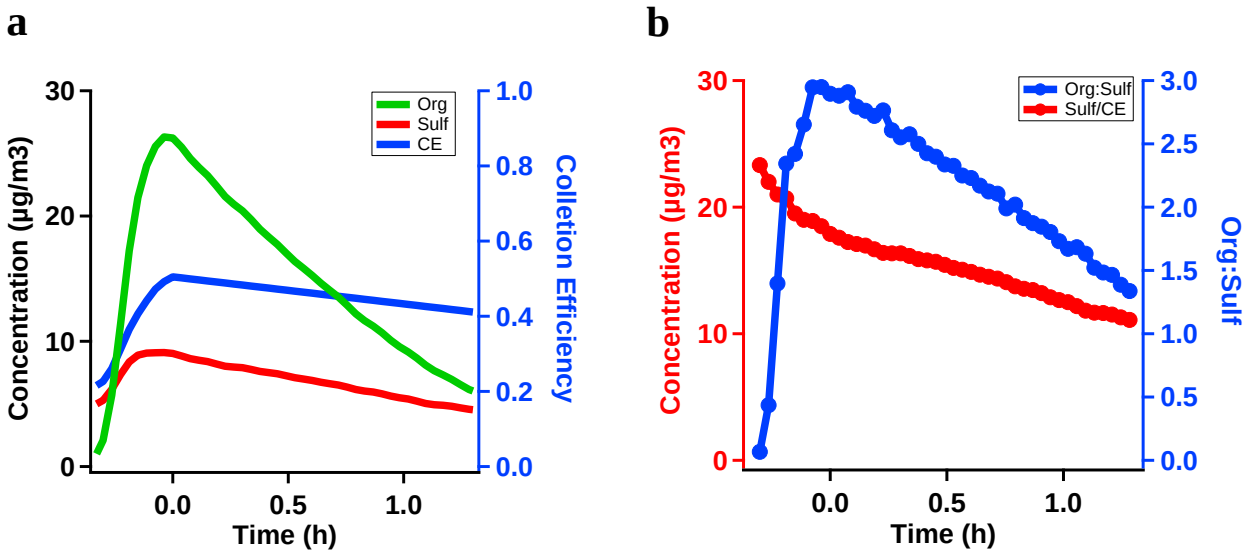

Figure 3.4 a. The organic and sulfate concentration and the collection efficiency measured with LS-HR-AMS. b. The corrected sulfate concentration and the org:sulf over the time.

Figure 3.5 shows the total wall loss of oleic acid (21 ^{o}C) and as well as levoglucosan (15 ^{o}C) vapor vs time. The results showed very good reproducibility. All six measurements of oleic acid and two measurements of levoglucosan matched with each other very well. The good linear correlation showed that the loss of oleic acid vapor to the Teflon chamber walls followed zeroth order kinetics as expected, and the vapor wall loss rate was constant. The constant vapor wall loss rate also indicated that the chamber walls were far from saturated. The loss rate was calculated using the slope, which was -15.8 ± 0.1 µg·m^{-3}·h^{-1} for oleic acid, and -11.4± 0.1 µg·m^{-3}·h^{-1} for levoglucosan. The saturation concentrations of oleic acid and levoglucosan are 4.0

μg·m^{-3} at 21 ^{o}C and 2.9 μg·m^{-3} at 15 ^{o}C, respectively. The loss rates are comparable to their saturation concentrations. The results showed that SVOCs with similar saturation concentrations had similar vapor wall rates. We also calculated the condensation sink to the chamber wall (CS^W) using Equation 6. The values from experiments with oleic acid and levoglucosan are almost identical, around 0.065 min^{-1}. It is about half of the value from sulfuric acid. Given the different time and measurement methods, this is good agreement. When comparing the condensation sink to the particles (CS^P), which is 1~2 min^{-1}, CS^P for the SVOCs is 15~30 times, much larger than CS^W. This confirms our initial hypothesis. The mass exchange of SVOCs between particles and vapor are much faster than the wall loss of vapor, and SVOC coated particles sustained SVOC vapors at or near to saturation concentration in the gas phase.

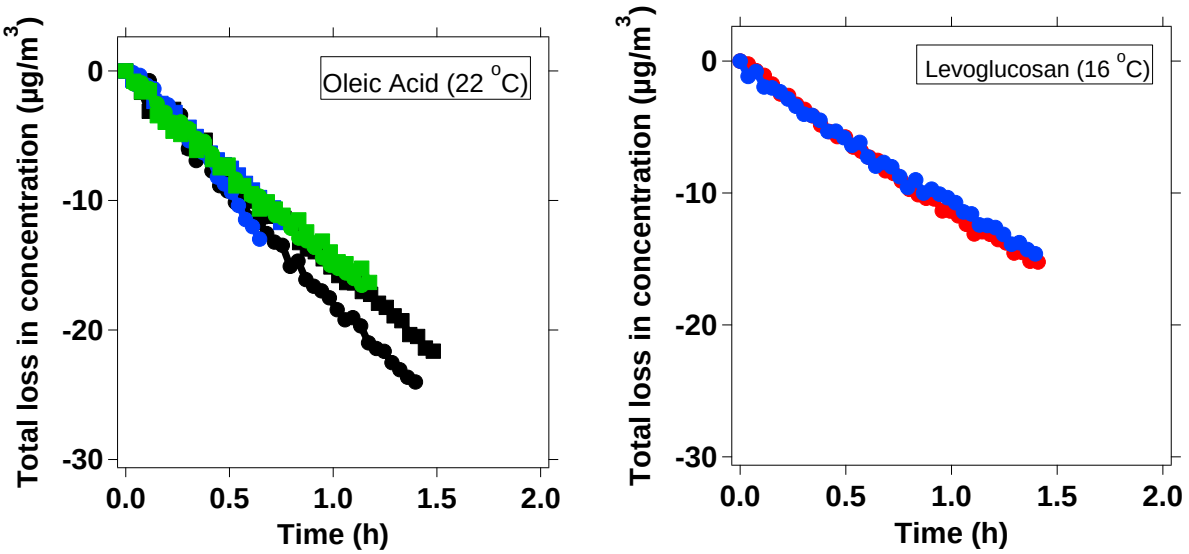

Figure 3.5 The total vapor loss of oleic acid and levoglucosan over the time.

3.3.6 The wall loss of oleic acid vapor with different molar fraction in oleic acid/d_{62}-squalane mixture.

To further investigate the relationship between vapor wall loss rate with the concentration of SVOC vapor in gas phase and the vapor wall behavior in mixture, we studied the wall loss of oleic acid vapor in oleic acid/d_{62}-squalane mixtures. For this experiment, we consider squlane to be nearly non-volatile. Following Raoult's law, the concentration of oleic acid vapor in the gas phase is proportional to its mole fraction in the mixture. We measured the vapor loss rate of oleic acid in a series of oleic acid/d_{62}-squalane mixtures with different molar fractions of oleic acid. The fragment $C_4D_9^+$ (m/z = 66) was used to calculate the concentration of d_{62}-squalane. The ratio of fragment $C_4D_9^+$ to d_{62}-squalane was 0.243 for pure d_{62}-squalane particles in the chamber. The fragments, $C_4H_7^+$ and $C_3H_3O^+$ (m/z = 55) were used to calculate the concentration of oleic acid. The ratio of both fragments ($C_4H_7^+$+ $C_3H_3O^+$) to oleic acid was 0.197 for pure oleic acid particles in the chamber. Figure 3.6 shows the total loss rate of oleic acid vapor over the time as a function of oleic acid molar fraction of in the mixture. We observed a higher loss rate of oleic acid when the mixture had higher molar fraction of oleic acid. Pure oleic acid showed a larger loss rate than in any mixture. This is due to the different vapor concentrations in the gas phase. The equilibrium vapor concentration was higher when there was more oleic acid in the mixture; pure oleic acid had the highest vapor concentration. The results demonstrate that the vapor wall loss rates were proportional to the concentrations of SVOC vapors in the gas phase.

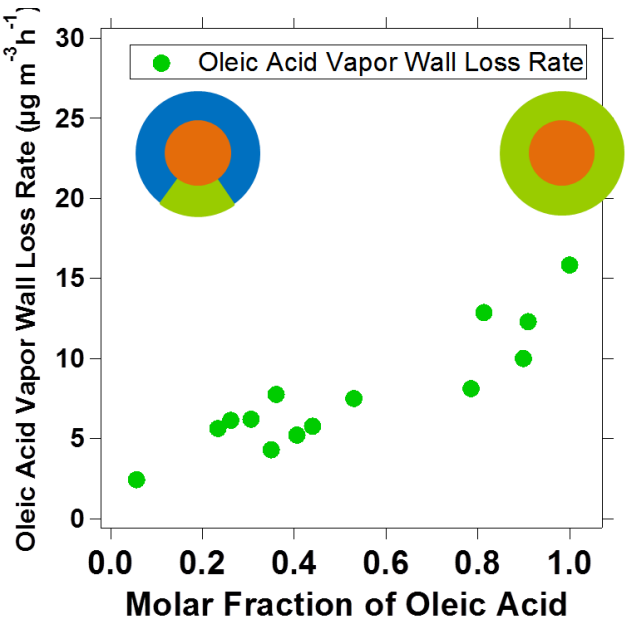

Figure 3.6 The wall loss rates of oleic acid vapor at different molar fraction in oleic acid/d_{62}-squalane mixture. The cartoon demonstrated the mass fraction of oleic acid (green) in the mixture of oleic acid (green)/d_{62}-squalane (blue) AS seeds is colored as red.

3.3.7 Observation of vapor wall loss of alkanes.

Figure 3.7 shows the change of org:sulf of ammonium sulfate particles coated by 4 alkanes, hexacosane, pentacosane, docosane and eicosane. The passive decay of alkanes started at time 0h. Hexacosane and pentacosane showed very small decreases of org:sulf. The org:sulf is almost a flat line over this period. Both docosane and eicosane showed steady decreases of org:sulf that indicated continuous vapor loss to the Teflon chamber wall. The org:sulf of eicosane decreased faster than docosane. Also, the org:sulf of eicosane almost reached 0 at the end of the experiment, which showed that all eicosane on the particles were gone, indicating that the SVOC vapors lost to the chamber wall were still far from saturating the chamber wall. The results clearly showed that the vapor wall loss of the alkanes increased with decreasing carbon number and increasing

the saturation concentration. Eicosane showed the largest loss rate; Hexacosane showed almost no wall loss.

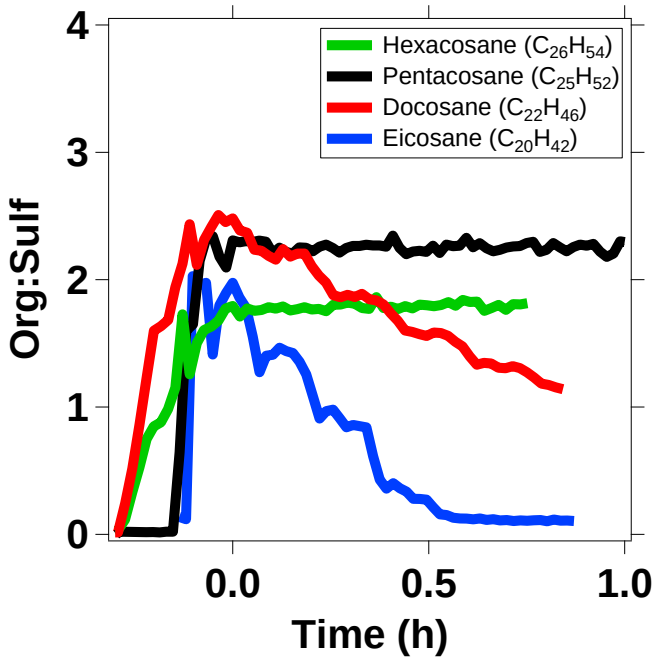

Figure 3.7 The change of org:sulf of ammonium sulfate particles coated by hexacosane, pentacosane, docosane and eicosane.

We summarize the vapor loss rate of all 7 SVOCs measured over their saturation concentration (Chickos and Hanshaw, 2003;May et al., 2012) in figure 3.8. It clearly shows that the wall loss rate of SVOCs vapor is significant and consistently proportional to the vapor concentrations in the gas phase. The wall loss of organic vapor needs to be considered in smog-chamber studies, especially when evaluating the SOA formation as well as OA evolution. However, this also suggests that the vapor wall loss of SVOCs may be practically irreversible under typical chamber SOA conditions, with single, chamber dependent wall condensation sink. This would greatly simplify wall loss corrections.

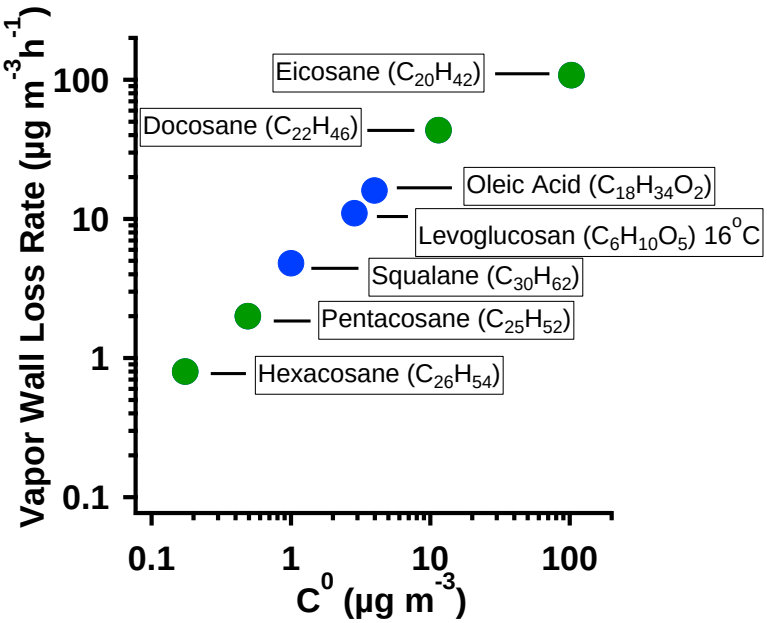

Figure 3.8 The vapor wall loss rates of hexacosane, pentacosane, docosane, eicosane, squalane, levoglucosan and oleic acid.

.

We can also address the question of whether organic vapor accommodation to the suspended particles is small, as suggested in a recent paper (Zhang et al., 2014a). Our results are consistent with the vapor-particle partitioning establishing a steady state far more rapidly than the vapor-wall exchange timescale, consistent with CS^P: CS^W > 10. One example is the rapid transition shown in figure 3.4b from an increasing Org:Sulf while oleic acid was being vaporized to a much slower decrease in Org:Sulf due to vapor wall loss. These data are consistent with others showing accommodation coefficient, α (org) > 0.1 (Saleh and Khlystov, 2009;Saleh et al., 2013;Julin et al., 2014). It is more difficult to assess the accommodation coefficient of organics to the Teflon wall, as vapor loss will be rate limited by diffusion for α (wall) > 1e-4 or so (McMurry and Grosjean, 1985). However, our results are consistent with α (wall) greater than this critical value.

3.4 Conclusions

We have successfully developed a method to constrain the vapor wall loss of SVOCs due to the adsorption and/or absorption of organic vapor to the Teflon chamber wall with a HR-ToF-AMS. The parameter org:sulf measured for coated particles can be used efficiently to determine if the vapor wall loss of SVOCs is significant. The loss rate of organic vapor to Teflon wall is proportional to both the decrease of Org:Sulf and the sulfate concentration, which can be calculated with the data from the HR-ToF-AMS measurement. Our results clearly demonstrate that the vapor wall loss rates of SVOCs are positively related to the SVOCs concentrations in the vapor phase. SVOCs with similar saturation concentration will have similar vapor wall loss rate. The loss rate will reduce when the SVOCs concentrations in the vapor phase decrease. Our results confirm that the vapor wall loss of organic vapor needs to be considered in smog-chamber study, especially when evaluating the secondary organic aerosol (SOA) formation from SVOCs as well as OA evolution.

3.5 References

Chickos, J. S., and Hanshaw, W.: Vapor Pressures and Vaporization Enthalpies of the n-Alkanes from C21 to C30 at T = 298.15 K by Correlation Gas Chromatography, Journal of Chemical & Engineering Data, 49, 77-85, 2003.

Donahue, N. M., Robinson, A. L., Stanier, C. O., and Pandis, S. N.: Coupled partitioning, dilution, and chemical aging of semivolatile organics, Environmental Science & Technology, 40, 2635-2643, 2006.

Ehn, M., Thornton, J. A., Kleist, E., Sipila, M., Junninen, H., Pullinen, I., Springer, M., Rubach, F., Tillmann, R., Lee, B., Lopez-Hilfiker, F., Andres, S., Acir, I.-H., Rissanen, M., Jokinen, T., Schobesberger, S., Kangasluoma, J., Kontkanen, J., Nieminen, T., Kurten, T., Nielsen, L. B., Jorgensen, S., Kjaergaard, H. G., Canagaratna, M., Maso, M. D., Berndt, T., Petaja, T., Wahner, A., Kerminen, V.-M., Kulmala, M., Worsnop, D. R., Wildt, J., and Mentel, T. F.: A large source of low-volatility secondary organic aerosol, Nature, 506, 476-479, 2014.

Grieshop, A. P., Miracolo, M. A., Donahue, N. M., and Robinson, A. L.: Constraining the Volatility Distribution and Gas-Particle Partitioning of Combustion Aerosols Using Isothermal Dilution and Thermodenuder Measurements, Environmental Science & Technology, 43, 4750-4756, 2009.

Hildebrandt, L., Donahue, N. M., and Pandis, S. N.: High formation of secondary organic aerosol from the photo-oxidation of toluene, Atmos. Chem. Phys., 9, 2973-2986, 2009.

Hoffmann, T., Odum, J. R., Bowman, F., Collins, D., Klockow, D., Flagan, R. C., and Seinfeld, J. H.: Formation of organic aerosols from the oxidation of biogenic hydrocarbons, J. Atmos. Chem. , 26, 189-222, 1997.

Julin, J., Winkler, P. M., Donahue, N. M., Wagner, P. E., and Riipinen, I.: Near-Unity Mass Accommodation Coefficient of Organic Molecules of Varying Structure, Environmental Science & Technology, 48, 12083-12089, 2014.

Kalberer, M., Paulsen, D., Sax, M., Steinbacher, M., Dommen, J., Prevot, A. S. H., Fisseha, R., Weingartner, E., Frankevich, V., Zenobi, R., and Baltensperger, U.: Identification of Polymers as Major Components of Atmospheric Organic Aerosols, Science, 303, 1659-1662, 2004.

Kamens, R., Jang, M., Chien, C.-J., and Leach, K.: Aerosol Formation from the Reaction of α-Pinene and Ozone Using a Gas-Phase Kinetics-Aerosol Partitioning Model, Environmental Science & Technology, 33, 1430-1438, 1999.

Kokkola, H., Yli-Pirilä, P., Vesterinen, M., Korhonen, H., Keskinen, H., Romakkaniemi, S., Hao, L., Kortelainen, A., Joutsensaari, J., Worsnop, D. R., Virtanen, A., and Lehtinen, K. E. J.: The role of low volatile organics on secondary organic aerosol formation, Atmos. Chem. Phys., 14, 1689-1700, 2014.

Loza, C. L., Chan, A. W. H., Galloway, M. M., Keutsch, F. N., Flagan, R. C., and Seinfeld, J. H.: Characterization of Vapor Wall Loss in Laboratory Chambers, Environmental Science & Technology, 44, 5074-5078, 2010.

Matsunaga, A., and Ziemann, P. J.: Gas-Wall Partitioning of Organic Compounds in a Teflon Film Chamber and Potential Effects on Reaction Product and Aerosol Yield Measurements, Aerosol Science and Technology, 44, 881-892, 2010.

May, A. A., Saleh, R., Hennigan, C. J., Donahue, N. M., and Robinson, A. L.: Volatility of organic molecular markers used for source apportionment analysis: Measurements and

implications for atmospheric lifetime, Environmental Science & Technology, 46, 12435-12444, 2012.

McMurry, P. H., and Grosjean, D.: Gas and aerosol wall losses in Teflon film smog chambers, Environmental Science & Technology, 19, 1176-1182, 1985.

McVay, R. C., Cappa, C. D., and Seinfeld, J. H.: Vapor-Wall Deposition in Chambers: Theoretical Considerations, Environmental Science & Technology, 48, 10251-10258, 2014.

Odum, J. R., Hoffmann, T., Bowman, F., Collins, D., Flagan, R. C., and Seinfeld, J. H.: Gas/particle partitioning and secondary organic aerosol yields, Environ. Sci. Technol., 30, 2580-2585, 1996.

Odum, J. R., Jungkamp, T. P. W., Griffin, R. J., Flagan, R. C., and Seinfeld, J. H.: The atmospheric aerosol-forming potential of whole gasoline vapor, Science, 276, 96-99, 1997.

Pandis, S. N., Paulson, S. E., Seinfeld, J. H., and Flagan, R. C.: Aerosol formation in the photooxidation of isoprene and β-pinene, Atmos. Environ., 25A, 997-1008, 1991.

Pankow, J. F.: An absorption model of gas/particle partitioning of organic compounds in the atmosphere, Atmos. Environ., 28, 185-188, 1994.

Pope, C. A., Ezzati, M., and Dockery, D. W.: Fine-Particulate Air Pollution and Life Expectancy in the United States, New England Journal of Medicine, 360, 376-386, 2009.

Presto, A. A., Huff Hartz, K. E., and Donahue, N. M.: Secondary organic aerosol production from terpene ozonolysis. 2. Effect of NO_x concentration, Environmental Science & Technology, 39, 7046-7054, 2005a.

Presto, A. A., HuffHartz, K. E., and Donahue, N. M.: Secondary organic aerosol production from terpene ozonolysis. 1. effect of UV radiation, Environ. Sci. Technol., 39, 7036-7045, 2005b.

Robinson, A. L., Donahue, N. M., Shrivastava, M. K., Weitkamp, E. A., Sage, A. M., Grieshop, A. P., Lane, T. E., Pierce, J. R., and Pandis, S. N.: Rethinking Organic Aerosols: Semivolatile Emissions and Photochemical Aging, Science, 315, 1259-1262, 2007.

Robinson, E. S., Saleh, R., and Donahue, N. M.: Organic aerosol mixing observed by single-particle mass spectrometry, The Journal of Physical Chemistry A, 117, 13935-13945, 2013.

Saleh, R., and Khlystov, A.: Determination of Activity Coefficients of Semi-Volatile Organic Aerosols Using the Integrated Volume Method, Aerosol Science and Technology, 43, 838-846, 2009.

Saleh, R., Donahue, N. M., and Robinson, A. L.: Time Scales for Gas-Particle Partitioning Equilibration of Secondary Organic Aerosol Formed from Alpha-Pinene Ozonolysis, Environmental Science & Technology, 47, 5588-5594, 2013.

Solomon, S. Q., D.; Manning, M.; Alley, R. B.; Berntsen, T.; Bindoff, N. L.; Chen, Z.; Chidthaisong, A.; Gregory, J. M.; Hegerl, G. C.: Climate change 2007: The physical science basis, contribution of working group 1 to the fourth assessment report of the Intergovernmental Panel on Climate Change, 2007.

Stanier, C. O., Donahue, N., and Pandis, S. N.: Parameterization of secondary organic aerosol mass fractions from smog chamber data, Atmospheric Environment, 42, 2276-2299, 2008.

Stern, J. E., Flagan, R. C., Grosjean, D., and Seinfeld, J. H.: Aerosol formation and growth in atmospheric aromatic hydrocarbon photooxidation, Environmental Science & Technology, 21, 1224-1231, 1987.

Trump, E. R., Riipinen, I., and Donahue, N. M.: Interactions between atmospheric ultrafine particles and secondary organic aerosol mass: a model study, Boreal Environ. Res., 19, 00-00, 2014.

Yeh, G. K., and Ziemann, P. J.: Alkyl Nitrate Formation from the Reactions of C8–C14 n-Alkanes with OH Radicals in the Presence of NOx: Measured Yields with Essential Corrections for Gas–Wall Partitioning, The Journal of Physical Chemistry A, 118, 8147-8157, 2014.

Zhang, Q., Jimenez, J. L., Canagaratna, M. R., Allan, J. D., Coe, H., Ulbrich, I., Alfarra, M. R., Takami, A., Middlebrook, A. M., Sun, Y. L., Dzepina, K., Dunlea, E., Docherty, K., DeCarlo, P. F., Salcedo, D., Onasch, T., Jayne, J. T., Miyoshi, T., Shimono, A., Hatakeyama, S., Takegawa, N., Kondo, Y., Schneider, J., Drewnick, F., Borrmann, S., Weimer, S., Demerjian, K., Williams, P., Bower, K., Bahreini, R., Cottrell, L., Griffin, R. J., Rautiainen, J., Sun, J. Y., Zhang, Y. M., and Worsnop, D. R.: Ubiquity and dominance of oxygenated species in organic aerosols in anthropogenically-influenced Northern Hemisphere midlatitudes, Geophys Res Lett, 34, L13801, 2007.

Zhang, S.-H., Shaw, M., Seinfeld, J. H., and Flagan, R. C.: Photochemical aerosol formation from α-pinene and β-pinene, J. Geophys. Res., 97(D18), 20717-20729, 1992.

Zhang, X., Cappa, C. D., Jathar, S. H., McVay, R. C., Ensberg, J. J., Kleeman, M. J., and Seinfeld, J. H.: Influence of vapor wall loss in laboratory chambers on yields of secondary organic aerosol, Proceedings of the National Academy of Sciences, 111, 5802-5807, 2014a.

Zhang, X., Schwantes, R. H., McVay, R. C., Lignell, H., Coggon, M. M., Flagan, R. C., and Seinfeld, J. H.: Vapor wall deposition in Teflon chambers, Atmos. Chem. Phys. Discuss., 14, 26765-26802, 2014b.

Chapter 4

Sorption of semi-volatile α-pinene SOA into non-volatile polyethylene glycol seeds

Abstract

Semi-volatile organic compounds (SVOCs) play an essential role in the formation and chemical ageing of secondary organic aerosol (SOA), and also the mixing of organic aerosol (OA) from different sources. Studying the sorption of SVOCs into particles is very important for understanding the potential contribution of SVOCs to the global aerosol budget. The gas-particle partitioning of SVOCs is influenced by the saturation concentration of the SVOCs, the total amount of OA and the viscosity of OA. Polyethylene glycol (PEG) seeds have unique properties and thus provide a new way to study the interaction between SVOCs with OA. The liquid morphology of PEG400 minimizes the effect of diffusivity, allowing SVOCs to reach equilibrium between gas phase and particle phase in a short time. PEG400 is nearly non-volatile, so it will not disturb the mass change in the particles or add extra species into gas phase. PEG400 is also a very good solvent for SVOCs based on the elemental oxygen to carbon ratio (~0.5). With a unique mass fragment $C_4H_9O_2^+$ (*m/z* = 89), PEG400 can easily be separated from α-pinene SOA in AMS. PEG400 is also relatively stable with OH radicals and O_3 present. Therefore, PEG400 may be used as seeds during the formation of SOA. The change in aerosol mass, size distribution, and particle composition confirmed the sorption of semi-volatile α-pinene SOA into PEG400 seeds. This also indicated that significant amount of SVOC vapors presented

in the gas phase after SOA formation. This is consistent with chemical ageing, mixing and other evolution of SOA in the atmosphere. Larger concentrations of SOA vapors were observed when SOA loadings were higher. With the similar loadings of SOA, the SOA formed from α-pinene reacted with HONO presented more SOA vapors, comparing to α-pinene reacted with ozone.

4.1 Introduction

Organic compounds comprise a large fraction particulate matter (PM) in the atmosphere. They makes up around 20–90% of the aerosol mass in the lower troposphere (Kanakidou et al., 2005). Secondary organic aerosol (SOA) accounts a significant fraction of the organic mass in PM (Zhang et al., 2007). Particulate matter has shown important impacts on human health and life expectancy (Pope et al., 2009) and also influences on Earth's climate by absorbing and scattering radiation (Solomon, 2007). A proper understanding the formation and evolution of organic aerosols is necessary to model their loading in the atmosphere more accurately. SOA formation usually starts with the oxidation of volatile organic compounds (VOCs), forming products of lower volatility that subsequently partition into the particle phase. SOA may also be formed from chemical reactions of organic compounds emitted originally in the condensed phase (Robinson et al., 2007). It has generally been thought that the most abundant oxidation products are semi-volatile organic compounds (SVOCs), which often exist in significant fractions in both condensed and vapor phases and continuously move between the two phases (Donahue et al., 2012b;Donahue et al., 2009;Donahue et al., 2006). However, Ehn at al recently suggested that extremely low-volatility organic compounds (ELVOCs) may contribute roughly two-thirds of the SOA mass (Ehn et al., 2014). ELVOCs form in the gas phase and condensed irreversibly onto aerosol surfaces to produce SOA.

Semi-volatile SOA vapors are thought to play essential roles in the formation of SOA, chemical aging and mixing processes. During and after SOA formation in the atmosphere, the organic compounds in the particle phase can cycle between the gas and particle phases (Seinfeld and Pankow, 2003;Donahue et al., 2006;Kroll and Seinfeld, 2008). The dynamic mass exchange between the gas and particle phases gradually changes the organic mass and the physical and chemical properties of aerosols. Semi-volatile organic compounds formed from different VOCs or in different locations may cross-partition between different types of organic aerosols based on their characteristics and perform the mass exchange between different OAs. The mixing process can increase the complexity of organic aerosols by adding more different organic species and increase the chances of chemical reaction inside the aerosols on the particles (Hildebrandt et al., 2011;Robinson et al., 2013). Chemical ageing, further reaction of first-generation oxidation products, makes the SOA vapors further oxygenated and often less volatile. This increases the organic aerosol mass (Donahue et al., 2012a;Henry and Donahue, 2012;Henry et al., 2012). Products with high oxidation state and low volatility will change the properties of aerosols. Heterogeneous oxidation by OH uptake is almost certainly a factor of 5–20 slower than the corresponding homogeneous oxidation due to gas-phase diffusion limitations (Lambe et al., 2009). Thus homogeneous oxidation of the SOA vapors is more important in the chemical ageing process when vapors are present.

Some products in the gas phase after SOA formation can be measured through Gas chromatography–mass spectrometry (GC-MS) (Jaoui et al., 2012). They can also been absorbed by filters or a denuder, following extraction with organic solvents (Böge et al., 2013). However, the extremely sticky, polar organics often do not elute from GC columns. Furthermore, we want to know what fraction of organic vapors can readily condense to particles. Here we provide a

new approach to investigate the semi-volatile SOA vapors from the perspective of particles. We use organic seeds with distinctive mass spectra as a sorptive "trap" for condensable organic vapors. Specifically, we used polyethylene glycol (PEG, MW=400) as an organic seeds/solvent to absorb the organic vapors in the gas phase and studied the trapped SOA vapors through the measurement of the particles. It can be considered as an extreme example of mixing, which forces SVOC vapors into the particle phase.

In this study, we describe experimental techniques for performing the sorption of semi-volatile α-pinene SOA into non-volatile PEG400 seeds and demonstrated the use of aerosol mass spectrometry (AMS) to determine the mass of SOA in the mixture of SOA and PEG400. We verified that PEG400 was a robust seed to study the SOA properties and formation even in the presence of oxidants. We were able to clearly separate the PEG400 mass spectra from α-pinene SOA based on unique fragments of the mass spectra measured by the AMS. We observed the uptake of α-pinene SOA vapors into PEG400 seeds and compared the difference between α-pinene SOA formed with OH and O_3 under different SOA loadings.

4.2 Materials and methods

Experiments were performed at the Carnegie Mellon University (CMU) Smog Chamber, a 10 m^3 Teflon bag suspended in a temperature controlled room. Many details of the experimental procedures were described in a previous paper (Hildebrandt et al., 2009). Only a brief description is provided here. Prior to experiments the chamber was cleaned by flushing with clean, dry air and exposed to high temperatures (~35 °C) and UV irradiation. After cleaning, the chamber was maintained at a constant temperature. Ammonium sulfate seeds ($(NH_4)_2SO_4$, Sigma Aldrich, 99.9 %) were formed by atomizing a 1 g/L solution of $(NH_4)_2SO_4$ in an ultrapure water

(Millipore) solution, then neutralizing and drying the particles before they entered the chamber. The PEG400 seeds were produced with a 5 g/L PEG400 solution in water following the same method for generating ammonium sulfate seeds. α-pinene (Sigma Aldrich, >99%) was added via a septum through which clean air passed to vaporize the terpene and carry it into the chamber. HONO was added to the chamber by bubbling filtered air through a nitrous acid solution for 20 min.

Particle number and volume distributions inside the chamber were measured using a scanning mobility particle sizer (SMPS, TSI classifier model 3080, CPC model 3772 or 3010). Particle mass was measured by a high resolution time-of-flight aerosol mass spectrometer (HR-ToF-AMS, Aerodyne Research, Inc.). Single-particle mass spectra for particles with Dva ≥180 nm were taken with an HR-ToF-AMS operated in light scattering single particle (LSSP) mode, which has been described in detail before (Robinson et al., 2013). We operated the HR-ToF-AMS according to the common protocol with the vaporizer temperature at 600 ^{o}C. We collected mass spectra and particle time-of-flight (pToF) measurements in V-mode. For all experiments, the HR-ToF-AMS alternated between V-mode and LSSP mode for 60s each.

4.3 Results and discussion

4.3.1 Verification of PEG400 as nearly non-volatile and stable seeds.

We selected PEG400 because it should be liquid (T_m= 4-8 °C) and above the glass transition (T_g= -63 °C), yet nearly non-volatile (C^*~10^{-4} μg m^{-3}, calculated following the literature) (Donahue et al., 2011). PEG400 should thus form nearly non-volatile seeds with high diffusivity. If there is any evaporation of PEG400 from particles, the organic mass observed on the particles would drop. Also, the composition would be altered. So firstly we tested PEG400 seeds for any

sign of evaporation. The method we used here is similar to what we used to trace the vapor loss of SVOC in chapter 3. We measured the mass change of organics (PEG400, green) and sulfate (red) on particles formed from a solution of PEG400 and AS with HR-AMS. The observations are shown in figure 4.1. The passive decay followed after the seeding step which was completed at 0h. The size distribution of PEG400 and sulfate from pToF measurement (figure 4.2) matched with each other very well. This indicates that the ratios of PEG400 and AS were almost same in every particle consistent with expectations. We used org:sulf from the AMS (blue) to determine if there was evaporation of PEG400 from particles. We did not observe any significant change in org:sulf during the experiment, which was indicated by the almost flat line (blue) in Figure 4.1. This means that PEG400 was nearly non-volatile as expected. The chamber temperature was increased to 40 ^{o}C after 1.3h (the vertical black line in Figure 4.1). We still did not observe any evaporation of PEG400 at 40 ^{o}C, even though the volatility of PEG400 became about a magnitude larger than at 22 ^{o}C. This further proved that PEG400 was nearly non-volatile even at elevated temperature.

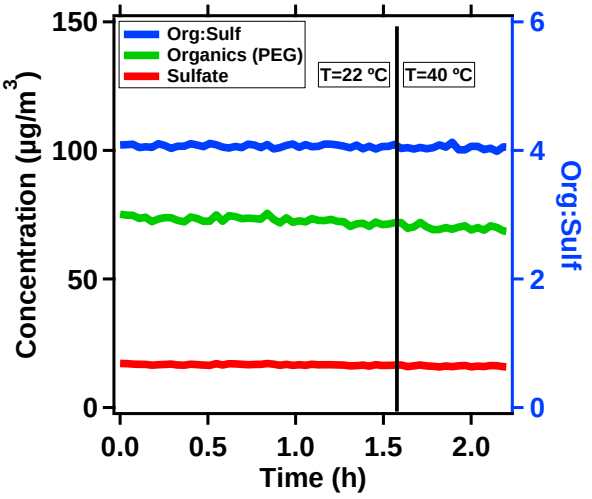

Figure 4.1 The organics (PEG400, green) and sulfates (red) concentration measured by HR-AMS at 22 ^{o}C and 40 ^{o}C. Org:sulf (blue) was the ratio of organics to sulfates concentrations.

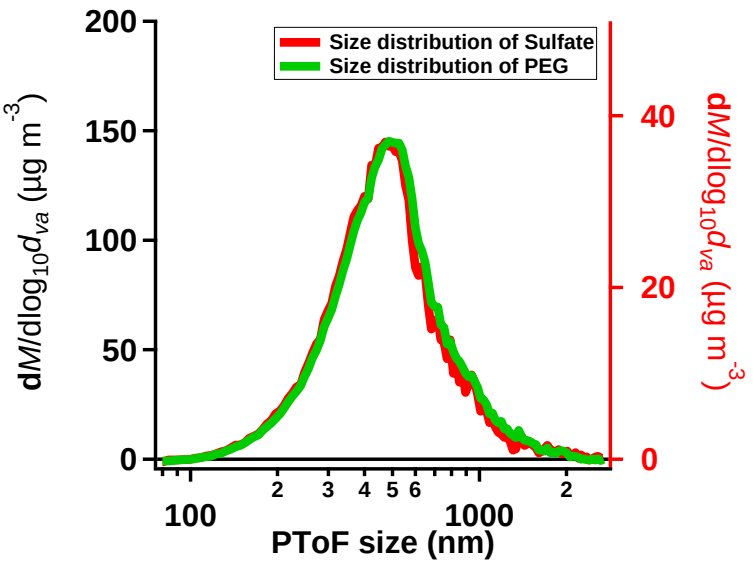

Figure 4.2 The size distribution of organics (PEG400) and sulfates measured by HR-AMS at 22 ^{o}C.

We also verified the chemical stability of PEG400. PEG400 does not have carbon-carbon double bonds (C=C) in its structure, therefore it should not react with ozone. However, it is not known whether it is relatively inert when OH radicals are present. If so, PEG400 can be used as seeds during SOA formation experiments. Figure 4.3 shows the mass change of PEG400 when there were OH radicals in the chamber. The injection of PEG400 coated AS particles was completed at time 0h. Photolysis of HONO started from the black line at 1.6h, with an estimated OH concentration of ~1e7 cm^{-3} for ~1h. At beginning of the experiment, the ratio of oxygen to carbon (O:C) and hydrogen to carbon (H:C) of PEG400 is around 0.5, 1.8, respectively, which is similar to the values calculated from its molecular structure. A very small increases of org:sulf (blue) was observed just after 1.6h, while the oxygen to carbon (O:C) and hydrogen to carbon (H:C) ratios slightly decreased. The coincidence of a mass increase of organics with a reduction in oxidation state suggests possible formation of a small amount of SOA from residual VOCs from previous experiments in the chamber. Although the results showed PEG400 may not be absolutely chemically inert to OH radicals, the change was nevertheless very small. Also, almost

no PEG400 vapors exist in the gas phase, so any oxidation of PEG400 with OH radicals was heterogeneous reaction, which was very slow. Figure 4.4 shows that the normalized mass spectra of PEG400 before (black) and organic particles after (blue) the oxidation were almost identical to each other. We further calculated the difference in the mass spectra before and after the oxidation (figure 4.5). We found that *m/z* = 41, 55 and 73 increased in the oxidation products. Overall, we believe it is possible to use PEG400 as seeds when studying SOA formation, although a very small fraction of PEG400 may react with OH radicals.

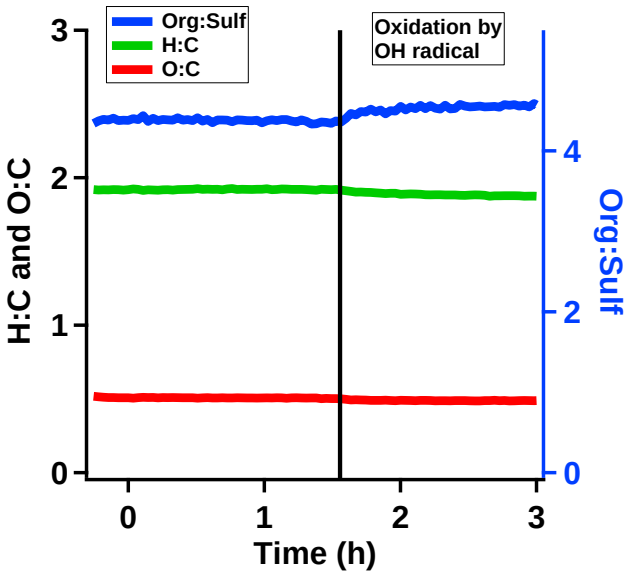

Figure 4.3 The change of org:sulf and the elemental composition, O:C and H:C, of PEG400 coated AS particle after introducing the OH radicals through photolysis of HONO in the chamber.

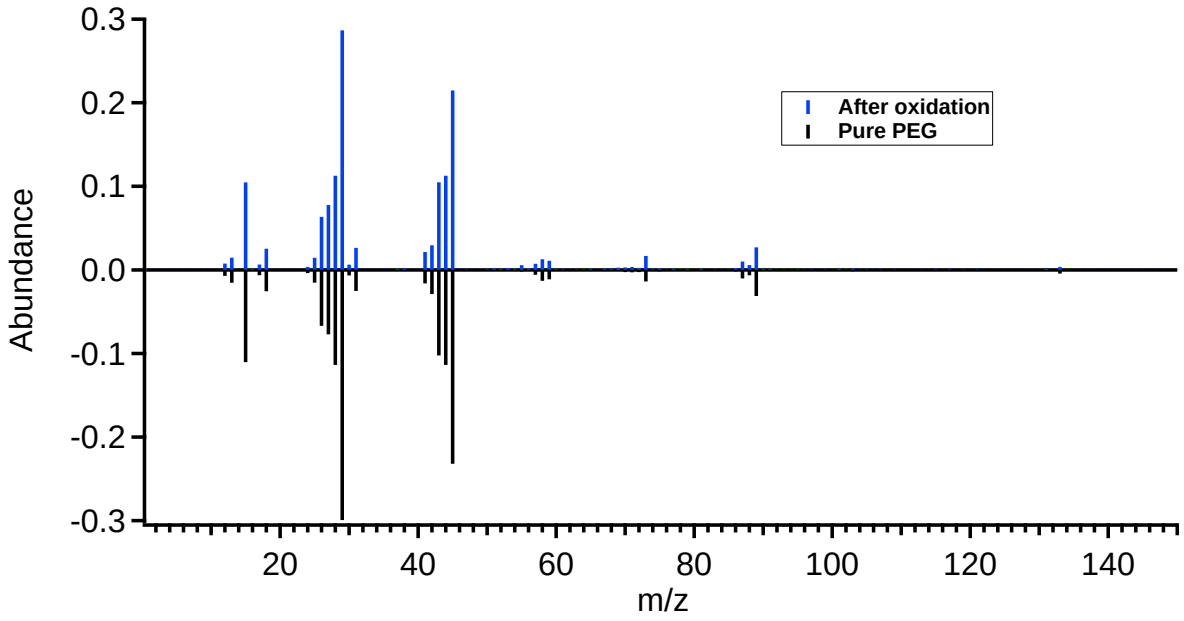

Figure 4.4 The normalized mass spectra of PEG400 before (black) and after (blue) the oxidation with OH radicals.

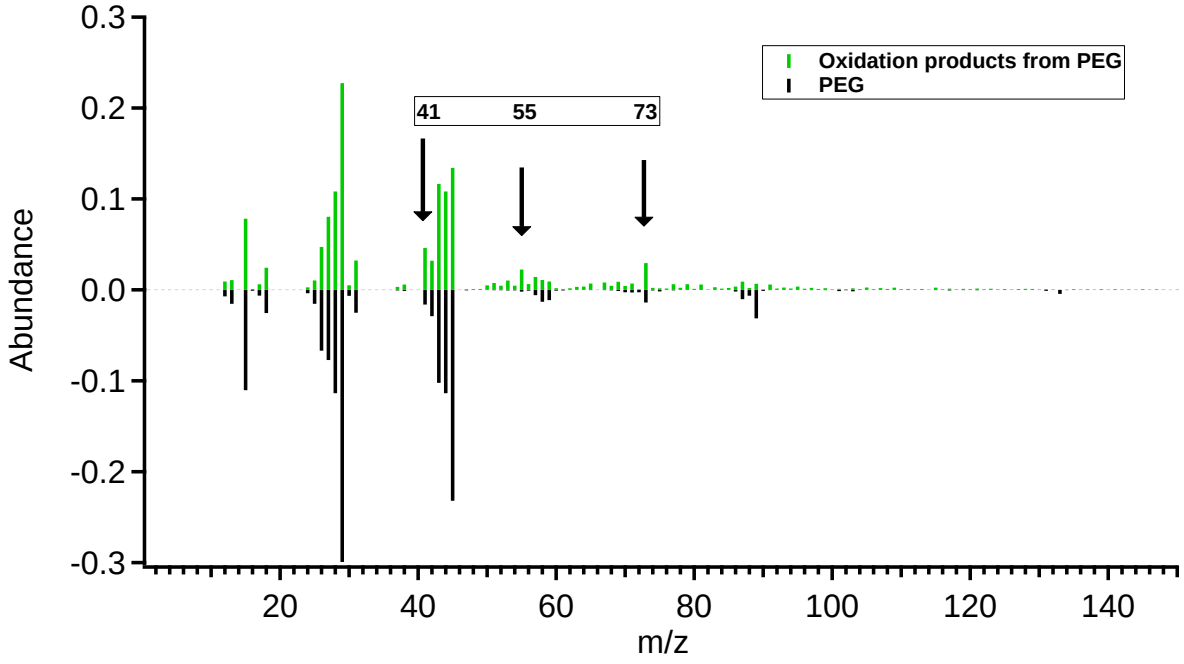

Figure 4.5 The normalized mass spectra of oxidation products from PEG400 with OH radicals (green), which was calculated as the difference of the mass spectra after and before the oxidation. The normalized mass spectra of pure PEG400 is shown as black.

4.3.2 Separation of signals on mass spectra coming from PEG400 or SOA.

Isotopic labeling is traditionally used to separate two organics. The *m/z* of ion fragments from deuterated compounds shift compared to normal compounds. For example, *m/z* =43, which is one of the most abundant peaks of SOA, mostly represents $C_2H_3O^+$. When normal hydrogen are replaced by deuterium, the deuterated ion fragment, $C_2D_3O^+$, shifts to *m/z* =46. Therefore, the deuterated SOA shows a major peak at *m/z* =46, instead of 43. Using *m/z* =46 as the unique fragment, it is possible to separate deuterated SOA from normal SOA. This method has been widely to use to study the mixing of SOAs and/or POAs. However, the challenge in this study was that we did not obtain either deuterium labeled α-pinene or PEG400. We tried to find other unique mass fragments for PEG400 and α-pinene SOA.

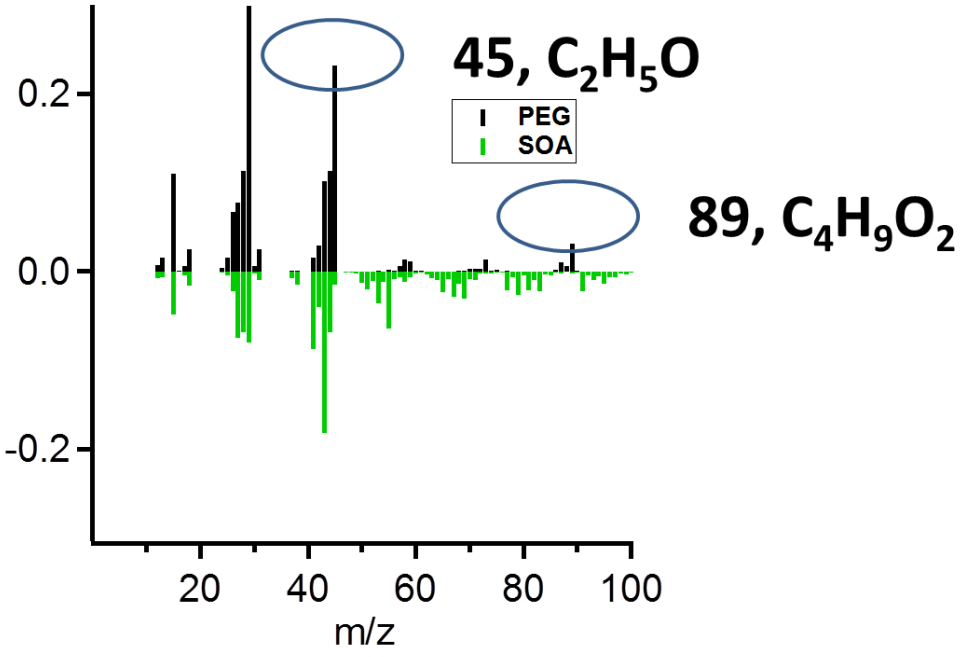

Figure 4.6 The normalized mass spectra of PEG400 before (black) and SOA (green).

As shown in figure 4.6, the most abundant peaks of PEG400 are *m/z* =29, 45 and 89. In the high resolution mass spectra of PEG400, $C_2H_5O^+$ and $C_4H_9O_2^+$, contributed to most of the signal at *m/z* =45 and 89. Both *m/z* 45 and 89 in the PEG400 spectra are around 10 times more prominent than in SOA, and can be used as unique tracers for PEG400. However, *m/z* 29 also shows very high abundance in SOA spectra and is thus not used. Since the concentration of each ion can be calculated from the measurement of HR-AMS, it is possible to separate SOA and PEG400 using their unique ion fragments more accurately.

Figure 4.7 compares the change of $C_2H_5O^+$ (left) and $C_4H_9O_2^+$ (right) concentrations before and after adding PEG400 into the chamber at time 0. Three different loadings of SOA were generated from the oxidation (OH or O_3) of 7.5, 75 and 150 ppbv of α-pinene, respectively. The same amount of PEG400 was used in all experiments. We compared the contribution of SOA to $C_2H_5O^+$ (left) and $C_4H_9O_2^+$ (right) after adding PEG400. When the SOA loading was low (blue, from 7.5ppbv of α-pinene), we observed that the contribution of SOA to $C_2H_5O^+$ and $C_4H_9O_2^+$ was negligible (< 1%). However, SOA contributed much more $C_2H_5O^+$ (left) than $C_4H_9O_2^+$ (right) when SOA loadings increased. At the highest SOA loading (red, from 150ppbv of α-pinene), the contribution of SOA to the total $C_4H_9O_2^+$ was only around 2%, but was 10% of the total $C_2H_5O^+$. Therefore, $C_4H_9O_2^+$ appeared to be a better tracer ion fragment. Based on the measurement from the HR-AMS, the mass fraction of $C_4H_9O_2^+$ in pure PEG400 spectra was 0.036. We used this value to convert the mass concentration of $C_4H_9O_2^+$ to the mass concentration of PEG400 added into the chamber.

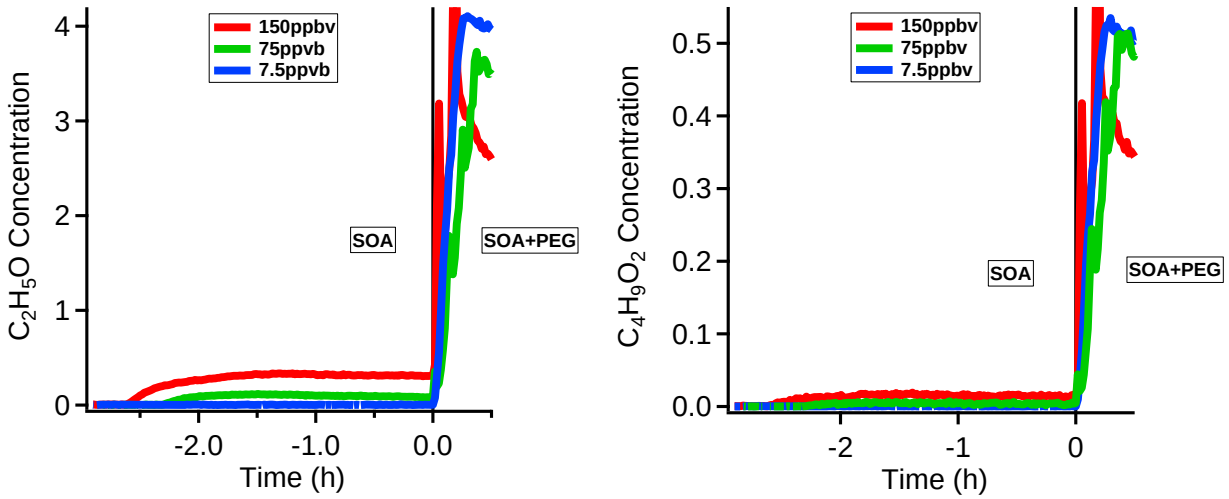

Figure 4.7 The difference of $C_2H_5O^+$ (left) and $C_4H_9O_2^+$ (right) concentration in α-pinene SOA after adding PEG400 at time 0h.

We also determined that *m/z* =67 ($C_5H_7^+$) was the unique mass fragment of α-pinene SOA compared to PEG400. We did not chose *m/z* =43 or 44, which are typically used as the characteristic peaks of α-pinene SOA, because they also showed large abundance in the PEG400 mass spectra. As shown in figure 4.8, there were almost no *m/z* 67 signals in the PEG400 mass spectra (black). *m/z* 67 had relatively high abundance in α-pinene SOA (green).

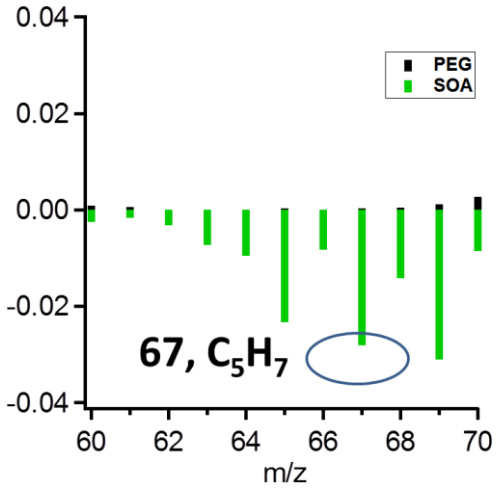

Figure 4.8 The normalized mass spectra of PEG400 (black) and SOA (green) only for *m/z* ranging from 60 to 70.

4.3.3 Sorption of semi-volatile SOA from α-pinene ozonolysis into PEG400.

SVOCs are major components of SOA, and their vapors should be significant in the gas phase. When PEG400, which is a good solvent for these vapors, is added into the chamber, SVOC vapors will be absorbed by PEG400 and the SOA mass will increase. To verify this hypothesis, we added PEG400 into the chamber after the SOA formation from α-pinene ozonolysis completed. As shown in figure 4.9, ammonium sulfate seeds (red) were introduced into the chamber at the beginning of the experiment. SOA formation from α-pinene ozonolysis started at around -3h. Pure PEG400 particles were added into the chamber at time 0h. We calculated the total amount of PEG400 based on the mass concentration of $C_4H_9O_2^+$. After subtracting the amount of PEG400 from the total organic mass, we obtained the total concentrations of SOA (blue). We found around 30% increase of SOA mass (blue) after PEG400 was added. This clearly indicates the sorption of semi-volatile vapors into PEG400 particles. We also heated up the chamber from 21 ^{o}C and 40 ^{o}C at 2.3h. The sharp decrease of organic and SOA mass in the next 20 mins suggested the evaporation of SOA, though from these data it is not possible to conclude whether evaporation occurred from AS seeds, PEG seeds or both.

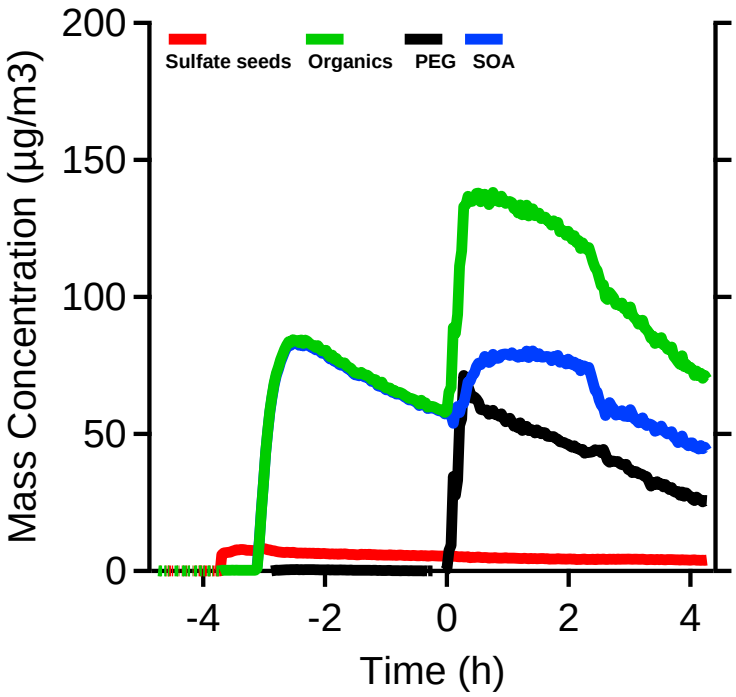

Figure 4.9 The organics and sulfate concentrations measured with HR-AMS. The PEG400 concentrations were calculated based on its unique fragment $C_4H_9O_2^+$. The concentrations of SOA (blue) were the difference between total organic and PEG400 concentrations.

Figure 4.10 shows the change in the size distribution of *m/z* =67 (green line), which is the unique mass fragment of SOA, from pToF measurements. Along with the increase in concentration, the size of particles containing *m/z* 67 also increased. PEG400 particles were larger than the SOA-coated AS particles. It is likely that SOA absorbing into PEG400 shifted the total distribution of *m/z* 67 to larger size.

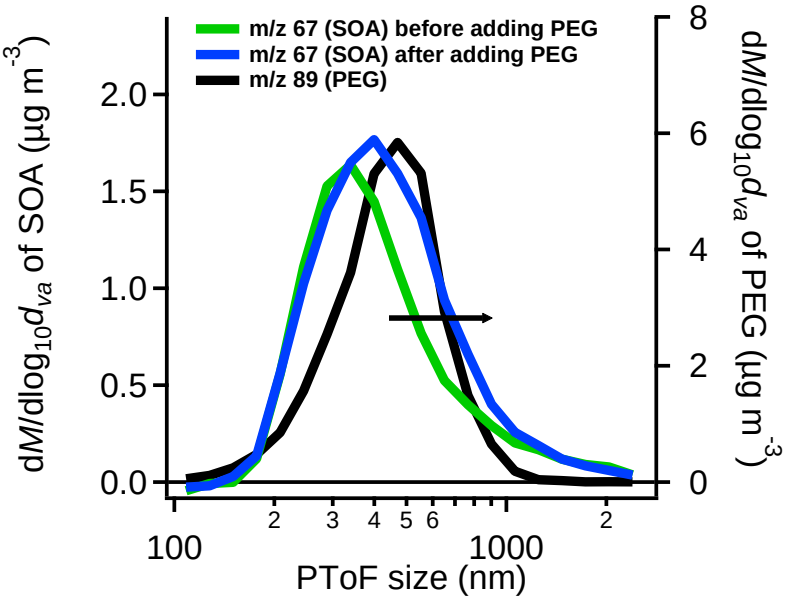

Figure 4.10 The size distribution of *m/z* 67, which is the unique mass fragment of α-pinene SOA, before (green) and after (blue) adding PEG400. The black is the sized distribution of *m/z* 89, which is the unique mass fragment of PEG400.

Single particle measurement provided additional evidence for the sorption of semi-volatile SOA into PEG400. Figure 4.11 shows the similarity of particles during the experiment to a reference spectrum, ammonium sulfate seeds coated by α-pinene SOA. The color scale shows the ratio of *m/z* =89 fragment in the organic mass (f89). Most of the *m/z* 89 signal came from PEG400. Pure PEG400 particles were measured separately in other experiments, and their similarity to the reference is shown in the inset at the lower left corner (black dots). The similarity of pure PEG400 seeds to the reference spectrum was only around 0.15. After PEG400 seeds were introduced into the chamber at time 0h, we observed particles located between pure PEG400 and SOA particles in the similarity plot. The particles in the middle had smaller f89 than the particles at the bottom. This clearly shows that the SOA vapors were absorbed into PEG400 particles, making the particles more similar to SOA and reducing the f89. Particles continued moving up

in the plot over time, indicating that they became more similar to the reference SOA. The particles can be separated into two different populations based on their seeds (i.e., ammonium sulfate or PEG400). Particles with *m/z* 80 were assumed to have ammonium sulfate as the seed, and particles with *m/z* 89 were assumed to have PEG400 as the seed. The red and black lines with dots show the evolution of these two populations by averaging particles in each population every 20mins. The increase of the SOA mass fraction in PEG400 (black) was due to the absorption of SOA vapors into PEG400. The mass fraction of SOA in the ammonium sulfate population decreased because of the evaporation of SOA. When heating up the chamber (black line), we observed a rapid decrease of the SOA mass fraction in both populations due to the evaporation of semi-volatile organics.

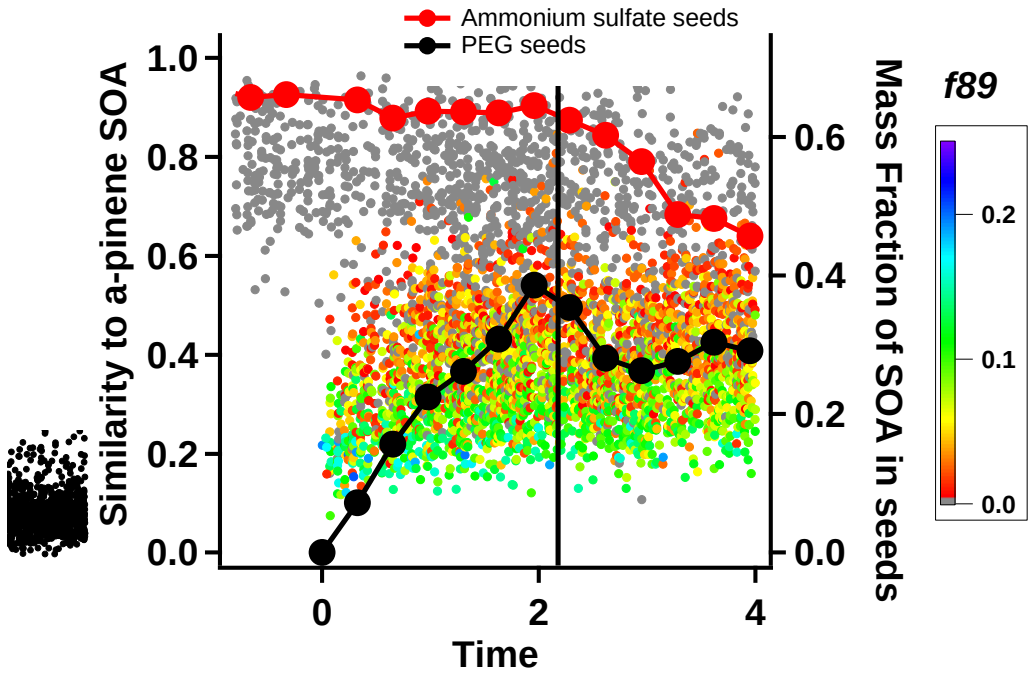

Figure 4.11 The similarity of particles to α-pinene SOA. The color scales showed the ratio of *m/z* 89 to the total organics in the particles (f89). The particles with f89<0.005 are colored as grey. The black dots shows pure PEG400 particles measured separately. The black line with the dots shows the mass fraction of SOA in PEG400 seeds. The red line with the dots shows the mass fraction of SOA on ammonium sulfate seeds.

4.3.4 Sorption of semi-volatile SOA from α-pinene reactions with HONO and ozone at three different loadings.

In order to investigate the relationship between the amount of semi-volatile SOA vapors and the suspended SOA concentration, we studied the sorption of SOA vapors into PEG400 for different initial concentrations of α-pinene (7.5, 75 and 150 ppbv) in the chamber. Also we compared the different effects of OH radicals and ozone. Figure 4.12 summarizes the mass fraction of SOA in the PEG400 seeds. The condensation sink the PEG400 seeds was around 0.08 min^{-1} based on the measurement in a separate experiment with the same injection setup and the same amount of PEG400, corresponding to a life time of 13 min (0.22h) for SOA condensation to the PEG. We therefore expect a roughly 13 min exponential approach to equilibrium for a purely sorptive process. The SOA mass fraction increased rapidly during the injection of PEG400, but slowed down over the time. The rapid increase at the beginning is broadly consistent with the expected equilibrium timescale; the slower tail may indicate another process. For both SOA prepared from α-pinene ozonolysis (left) and reaction with HONO (right), we observed higher mass fraction of SOA in PEG400 when SOA loadings were higher. This can also be seen in figure 4.13 which shows the relationship between the mass fractions of SOA in the PEG400 population and the total SOA concentration at time 0h. We also observed that the SOA mass fractions in PEG400 were higher in experiments with α-pinene and HONO than experiments with α-pinene and ozone. This is consistent with observations that the SOA yields from α-pinene reacted with OH were usually lower than ozonolysis. This is because SOA formed from α-pinene oxidation with OH was more volatile due to the formation of organic nitrate.

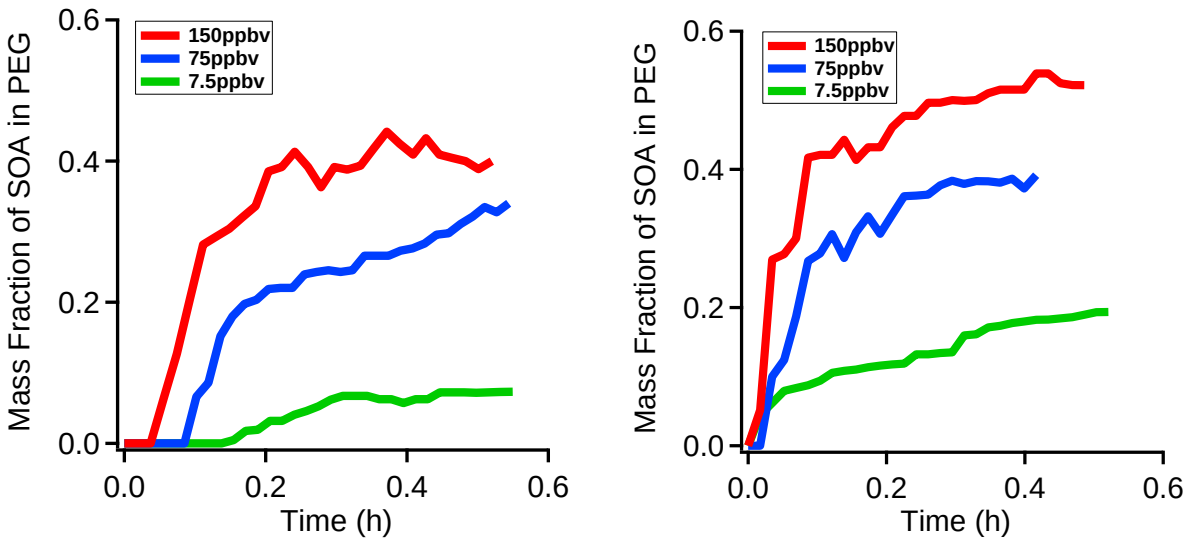

Figure 4.12 Mass fraction of SOA from α-pinene ozonolysis (left) and α-pinene reacted with OH (right) in PEG400 population. The initial α-pinene concentration were 150 (red), 75 (blue) and 7.5 ppbv (green).

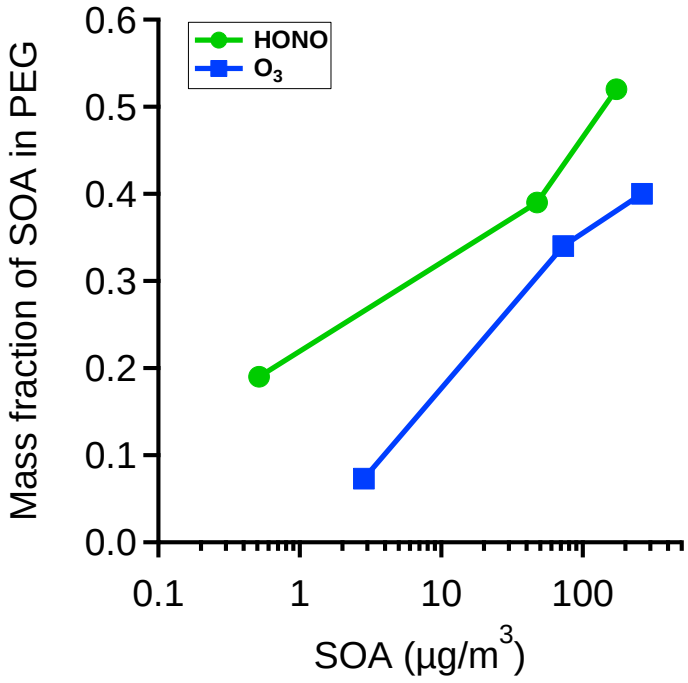

Figure 4.13 The relationship between mass fraction of SOA from α-pinene ozonolysis and α-pinene reacted with OH in PEG400 population vs the SOA concentration just before adding PEG400.

4.4 Conclusion

PEG400 may be a very good organic seed with special prosperities, liquid, water-soluble, nearly non-volatile, good solvent for SOA and relative stable during the oxidation with OH radicals and ozone. PEG400 can be easily separated from the SOA mass spectrum with the unique fragment $C_4H_9O_2^+$ at *m/z* =89. Significant sorption of semi-volatile α-pinene SOA into PEG400 was proved consistently through the analysis of SOA mass increase, shift of size distribution and single particles composition. The results demonstrated that SOA prepared from α-pinene reacted with OH produced more semi-volatile SOA vapors comparing to α-pinene ozonolysis. More semi-volatile SOA vapors were observed in the gas phase with higher SOA loadings. This method allows further investigation the properties, such as volatility and composition, of semi-volatile SOA vapors using the measurement methods for particles.

4.5 References

Böge, O., Mutzel, A., Iinuma, Y., Yli-Pirilä, P., Kahnt, A., Joutsensaari, J., and Herrmann, H.: Gas-phase products and secondary organic aerosol formation from the ozonolysis and photooxidation of myrcene, Atmospheric Environment, 79, 553-560, 2013.

Donahue, N. M., Robinson, A. L., Stanier, C. O., and Pandis, S. N.: Coupled partitioning, dilution, and chemical aging of semivolatile organics, Environmental Science & Technology, 40, 2635-2643, 2006.

Donahue, N. M., Robinson, A. L., and Pandis, S. N.: Atmospheric organic particulate matter: From smoke to secondary organic aerosol, Atmospheric Environment, 43, 94-106, 2009.

Donahue, N. M., Epstein, S. A., Pandis, S. N., and Robinson, A. L.: A two-dimensional volatility basis set: 1. organic-aerosol mixing thermodynamics, Atmos. Chem. Phys., 11, 3303-3318, 2011.

Donahue, N. M., Henry, K. M., Mentel, T. F., Kiendler-Scharr, A., Spindler, C., Bohn, B., Brauers, T., Dorn, H. P., Fuchs, H., Tillmann, R., Wahner, A., Saathoff, H., Naumann, K.-H., Möhler, O., Leisner, T., Müller, L., Reinnig, M.-C., Hoffmann, T., Salo, K., Hallquist, M., Frosch, M., Bilde, M., Tritscher, T., Barmet, P., Praplan, A. P., DeCarlo, P. F., Dommen, J., Prévôt, A. S. H., and Baltensperger, U.: Aging of biogenic secondary organic aerosol via gas-phase OH radical reactions, PNAS, 109, 13503-13508, 2012a.

Donahue, N. M., Kroll, J. H., Pandis, S. N., and Robinson, A. L.: A two-dimensional volatility basis set – Part 2: Diagnostics of organic-aerosol evolution, Atmos. Chem. Phys., 12, 615-634, 2012b.

Ehn, M., Thornton, J. A., Kleist, E., Sipila, M., Junninen, H., Pullinen, I., Springer, M., Rubach, F., Tillmann, R., Lee, B., Lopez-Hilfiker, F., Andres, S., Acir, I.-H., Rissanen, M., Jokinen,

T., Schobesberger, S., Kangasluoma, J., Kontkanen, J., Nieminen, T., Kurten, T., Nielsen, L. B., Jorgensen, S., Kjaergaard, H. G., Canagaratna, M., Maso, M. D., Berndt, T., Petaja, T., Wahner, A., Kerminen, V.-M., Kulmala, M., Worsnop, D. R., Wildt, J., and Mentel, T. F.: A large source of low-volatility secondary organic aerosol, Nature, 506, 476-479, 2014.

Henry, K. M., and Donahue, N. M.: Photochemical aging of α-pinene secondary organic aerosol: Effects of OH radical sources and photolysis, The Journal of Physical Chemistry A, 2012.

Henry, K. M., Lohaus, T., and Donahue, N. M.: Organic aerosol yields from α-pinene oxidation: Bridging the gap between first-generation yields and aging chemistry, Environmental Science & Technology, 46, 12347-12354, 2012.

Hildebrandt, L., Donahue, N. M., and Pandis, S. N.: High formation of secondary organic aerosol from the photo-oxidation of toluene, Atmos. Chem. Phys., 9, 2973-2986, 2009.

Hildebrandt, L., Henry, K. M., Kroll, J. H., Worsnop, D. R., Pandis, S. N., and Donahue, N. M.: Evaluating the mixing of organic aerosol components using high-resolution aerosol mass spectrometry, Environmental Science & Technology, 45, 6329–6335, 2011.

Jaoui, M., Kleindienst, T. E., Offenberg, J. H., Lewandowski, M., and Lonneman, W. A.: SOA formation from the atmospheric oxidation of 2-methyl-3-buten-2-ol and its implications for PM2.5, Atmos. Chem. Phys., 12, 2173-2188, 2012.

Kanakidou, M., Seinfeld, J. H., Pandis, S. N., Barnes, I., Dentener, F. J., Facchini, M. C., Dingenen, R. V., Ervens, B., Nenes, A., Nielsen, C. J., Swietlicki, E., Putaud, J. P., Balkanski, Y., Fuzzi, S., Horth, J., Moortgat, G. K., Winterhalter, R., Myhre, C. E. L., Tsigaridis, K., Vignati, E., Stephanou, E. G., and Wilson, J.: Organic aerosol and global climate modelling: a review, Atmos. Chem. Phys., 5, 1053-1123, 2005.

Kroll, J. H., and Seinfeld, J. H.: Chemistry of secondary organic aerosol: Formation and evolution of low-volatility organics in the atmosphere, Atmos. Environ., 42, 3593, 2008.

Lambe, A. T., Miracolo, M. A., Hennigan, C. J., Robinson, A. L., and Donahue, N. M.: Effective Rate Constants and Uptake Coefficients for the Reactions of Organic Molecular Markers (n-Alkanes, Hopanes, and Steranes) in Motor Oil and Diesel Primary Organic Aerosols with Hydroxyl Radicals, Environmental Science & Technology, 43, 8794-8800, 2009.

Pope, C. A., Ezzati, M., and Dockery, D. W.: Fine-Particulate Air Pollution and Life Expectancy in the United States, New England Journal of Medicine, 360, 376-386, 2009.

Robinson, A. L., Donahue, N. M., Shrivastava, M. K., Weitkamp, E. A., Sage, A. M., Grieshop, A. P., Lane, T. E., Pierce, J. R., and Pandis, S. N.: Rethinking organic aerosols: Semivolatile emissions and photochemical aging, Science, 315, 1259-1262, 2007.

Robinson, E. S., Saleh, R., and Donahue, N. M.: Organic aerosol mixing observed by single-particle mass spectrometry, The Journal of Physical Chemistry A, 117, 13935-13945, 2013.

Seinfeld, J. H., and Pankow, J. F.: Organic atmospheric particulate materal, Annual Review of Physical Chemistry, 54, 121-140, 2003.

Solomon, S. Q., D.; Manning, M.; Alley, R. B.; Berntsen, T.; Bindoff, N. L.; Chen, Z.; Chidthaisong, A.; Gregory, J. M.; Hegerl, G. C.: Climate change 2007: The physical science basis, contribution of working group 1 to the fourth assessment report of the Intergovernmental Panel on Climate Change, 2007.

Zhang, Q., Jimenez, J. L., Canagaratna, M. R., Allan, J. D., Coe, H., Ulbrich, I., Alfarra, M. R., Takami, A., Middlebrook, A. M., Sun, Y. L., Dzepina, K., Dunlea, E., Docherty, K., DeCarlo, P. F., Salcedo, D., Onasch, T., Jayne, J. T., Miyoshi, T., Shimono, A., Hatakeyama, S., Takegawa, N., Kondo, Y., Schneider, J., Drewnick, F., Borrmann, S., Weimer, S., Demerjian,

K., Williams, P., Bower, K., Bahreini, R., Cottrell, L., Griffin, R. J., Rautiainen, J., Sun, J. Y., Zhang, Y. M., and Worsnop, D. R.: Ubiquity and dominance of oxygenated species in organic aerosols in anthropogenically-influenced Northern Hemisphere midlatitudes, Geophys Res Lett, 34, L13801, 2007.

Chapter 5

Summary and outlook

5.1 Organic vapor chamber walls interaction.

As demonstrated in chapter 2 and 3, the Teflon chamber walls can adsorb or absorb organic vapors. The vapor loss of organic species reduces the observed SOA mass yield. In chapter 2, the loss of the SOA precursors has been measured by comparing the total injected organic to the vapor concentration in the gas phase, which was measured by GERSTEL thermal desorption gas chromatography. In chapter 3, the wall loss behaviors of several semi-volatile organic compounds have been studied, which are the preliminary results to explore the vapor wall loss of semi-volatile oxidation products during SOA formation. The following subjects may be helpful to understand more about the vapor wall loss.

5.1.1 Vapor wall loss of SOA with monodispersed seeds.

Aerosols with deferent sizes and shapes may show the different particle wall deposition rates. When using ammonium sulfate as seeds to prepare SOA, the smaller particles usually have larger organic mass fraction. Then the different wall loss rate between smaller and larger particles may change the ratio of total organic to sulfate mass. The effect is very small compared to the change due to vapor wall loss as discussed in chapter 3. Monodispersed seeds will be very useful to minimize this uncertainty. The new instrument, condensation monodisperse aerosol generator 3475 (CMAG), can be used to accomplish it. The wall loss behaviors of several semi-volatile surrogates have been studies in chapter 3. It will be very useful to expand the study to the real SOA system. The similar method will be used. Monodispersed seeds generated from CMAG will

be used to minimize the effect of size dependent particle wall loss. The vapor loss behaviors of different type and loadings of SOA may be studied. This study may constrain the vapor loss of semi-volatile oxidation products during SOA formation, which is helpful to get more accurate SOA yields.

5.1.2 Model study of SOA formation when considering vapor wall loss.

The wall deposition of the organics, either the precursors or the products, reduced the SOA mass yield observed in Teflon chamber. The next question is how large is the effect. The model simulation may be one approach to investigate the effect. One possible way is adding the vapor wall loss rate into the model, which was measured in chapter 3, based the volatility of several SVOCs. The volatility basic set (VBS) may be used to determine organic concentration in the gas phase in each volatility bin and then to determine the wall loss of the vapors.

5.2 Understanding the properties, behaviors of organic species in GAS phase.

The oxidation products in the gas phase formed during SOA formation are very important, which may undergo further reaction, or mass exchange between different aerosols. The aerosol research community has established systematic methods to study the particles, such as size, chemical composition, optical properties, climate and health effects. Studying organic vapors in the gas phase by measuring particle was deployed in this thesis, which includes measuring the mass loss of organics from particles and inferring to the loss of organic vapors in the gas phase (chapter 3), and trapping the semi-volatile SOA vapors into the particle and studying their properties through measuring the particles (chapter 4). These provide a new approach to study the oxidation products in the gas phase, "studying vapors via particles." While, direct measurements are always the key to build up the knowledge on all organic species in the gas phase.

5.2.1 Comparing the difference of SOA vapor absorbed by PEG seeds with normal SOA.

Chapter 4 showed that PEG400 may be good seeds to study SOA formation and properties. Significant amount of SOA vapors present in the gas phase can be absorbed by PEG seeds. Future study may focus on analyzing the properties of the absorbed SOA vapors in PEG and comparing them to the SOA in the particle phase. The volatility distribution can be studied with a thermal denuder. Further analysis of AMS data may give more information about the chemical compositions of the absorbed SOA vapors. The difference between SOA vapors and SOA in the particles may be helpful to understand mixing, ageing and other evolution processes.

5.2.2 Studying the organic species with Chemical Ionization with the Atmospheric Pressure interface Time-Of-Flight mass spectrometer (CI-APi-TOF).

Direct measurement of organic species in the gas phase is essential to know what is and what is happening in the gas phase during SOA formation. CI-APi-TOF is a reliable and highly sensitive tool for measurements of low concentrations of molecules and clusters. High mass resolution of the APi-TOF was crucial in the separation of the oxidation products which includes more than thousands of compounds. CI-APi-TOF may be capable to measure the total organic species, and also trace the concentration change of the chosen compounds. CI-APi-TOF may be helpful to track the production, the condensation and also the vapor wall loss of one specific oxidation product during SOA formation. This may help to explain the difference of SOA mass yields between chamber results and field measurements.